

REMOTE SENSING EVAPOTRANSPIRATION (SEBS) EVALUATION USING WATER BALANCE

Report to the
Water Research Commission

by

Lesley Gibson¹, Zahn Münch², Marilie Carstens³ & Julian Conrad³

¹ARC – Agricultural Research Council – Institute for Soil, Climate and Water,
Stellenbosch

²CGA – Centre for Geographical Analysis, Stellenbosch University

³GEOSS – Geohydrological and Spatial Solutions International (Pty) Ltd,



WRC Report No. KV 272/11
ISBN 978-1-4312-0120-4

June 2011

The publication of this report emanates from a project entitled *Remote sensing evapotranspiration (SEBS) evaluation using water balance* (WRC Project No. K8/929/1)

DISCLAIMER

This report has been reviewed by the Water Research Commission (WRC) and approved for publication. Approval does not signify that the contents necessarily reflect the views and policies of the WRC, nor does mention of trade names or commercial products constitute endorsement or recommendation for use.

Executive Summary

This report follows on from WRC Report 1690/1/09 (Gibson *et al.*, 2009) entitled "Remote sensing as a tool for resource assessment towards the determination of the legal compliance of surface and groundwater use" which showed that due to many uncertainties and limitations with both the input data and methodology, it was not possible to determine the actual water consumption of individual farms or compliance to legislation. In this project, the aim was to address the uncertainties and limitations in WRC Report 1690/1/09 and thereby determine the efficacy or inefficiency of the method to highlight water-stressed catchments.

The bulk of the research effort in this project has been on the *ET* component using the SEBS model which is available as open-source freeware and therefore tempting to use by practitioners with remote sensing knowledge who may not necessarily have the micrometeorological expertise to develop a model themselves to estimate *ET*. However, the derivation of *ET* using the SEBS model is a complex process requiring several sources of input data and numerous processing steps to derive intermediate output products. The intermediate products are then combined through additional processing algorithms to derive the final daily *ET* product. Whilst the open-source format of SEBS is very useful and can speed up the research process, there are some instances where specialist knowledge is required to implement the model correctly to derive the most accurate results. For this reason, in this research the potential sources of error in the operating of the SEBS model are highlighted, the propagation of these errors through the model are illustrated and recommendations are made regarding the choice of input data and formulae. Finally the methodology used in Gibson *et al.* (2009) is modified to minimize the sources of error which were highlighted.

The study focuses on two quaternary catchments with different hydrological regimes that were selected on the basis of the availability of data and the characteristics of the landscapes, in order to test the *ET* methodology, in two different scenarios – one where water availability is limited but energy is not and one where water availability is less of a constraint in times where energy is not a limiting factor. Despite the modifications to reduce uncertainties, and the selection of homogeneous catchments, as with the results of Gibson *et al.* (2009), the SEBS model appears to overestimate catchment *ET*. In most cases the SEBS *ET* results do not appear to reflect limits in

water availability and ET is simply highest when the energy or atmospheric demand is the highest and lowest where the energy or atmospheric demand is the lowest, regardless of the accuracy of the input data, the hydrological regime and the environment. It is believed that the overestimation in ET is caused by the sensitivity of H to T_0-T_a and z_0 , both separately and in combination, particularly at high T_0-T_a and z_0 . This sensitivity to T_0-T_a is particularly important with respect to image selection, including the time of day of image acquisition, as the differential heating of the land surface and the air will determine the magnitude and sign of T_0-T_a .

An alternative method to calculate ET from remotely sensed data referred to as the ET-API method returned more realistic results for both the selected catchments but in the absence of field validation data the absolute accuracy of this model could not be determined. The trend of the ET-API method over the study period was more favourable in that it reflected both the availability of energy and the availability of water with peaks in precipitation during the dry season being reflected in the ET-API results.

The response of the differing water balance components (rainfall, groundwater and soil moisture) over the study period showed that the results of the different methodologies agree in terms of the trends that they highlight. The ARC-ISCW grid predicted catchment rainfall with a high degree of accuracy although the number of validation stations was limited. From the cumulative rainfall and ET results in G30G, the higher than rainfall ET results could indicate water stress. From this study it can be concluded that ET (ET-API) and precipitation methodologies presented may be used quantitatively for a water balance study at quaternary catchment scale. SHARE soil moisture data, which gives an indication of the relative soil moisture rather than a quantity of water stored in the soil, gave promising results and can be used to assess the reliability of the ET results by indicating the availability of water. Water levels where available are more difficult to incorporate since they represent point locations and are not necessarily representative of a catchment. Finally, the shortage of river gauges makes the incorporation of runoff data difficult.

The recommendations from this study include:

- Investigation of improved parameterization for the SEBS model by the model developers for ET calculations in vegetation with higher canopies.

- Additional research effort into the ET-API method.
- Research into the influence of time of day of satellite acquisition on land surface air temperature gradient.
- A methodology to produce accurate roughness lengths.
- Application of SHARE soil moisture data at catchment scale

Table of Contents

Table of Contents	vi
List of Figures	vii
List of Tables	ix
Acronyms/Abbreviations	x
Acknowledgments.....	xii
Chapter 1 – Introduction	1
Chapter 2 – Study area selection.....	6
Chapter 3 – Study area description	11
Chapter 4 – Evapotranspiration	15
Chapter 5 – Precipitation	45
Chapter 6 – Groundwater.....	49
Chapter 7 – Soil moisture	54
Chapter 8 – Runoff.....	58
Chapter 9 – Water balance.....	61
Chapter 10 – Conclusions and Recommendations.....	66
References:.....	70
APPENDIX 1 – P10A field campaign.....	74

List of Figures

<i>Figure 2.1: Selection of quaternary catchments for each hydrological regime</i>	<i>7</i>
<i>Figure 2.2: Percentage of landcover class per MODIS pixel in G30G (A) and P10A (B)</i>	<i>9</i>
<i>Figure 4.1: An example of top of atmosphere radiation versus surface shortwave radiation at the same location</i>	<i>22</i>
<i>Figure 4.2: Image date selection for G30G.....</i>	<i>23</i>
<i>Figure 4.3: Image date selection for P10A.</i>	<i>24</i>
<i>Figure 4.4: NDVI values for the P10A catchment across the study period.....</i>	<i>26</i>
<i>Figure 4.5: Difference in sensible heat flux results when using the LAI or NDVI approach to calculate the fractional vegetation cover.</i>	<i>27</i>
<i>Figure 4.6: The combined effect of T_0-T_a and landcover on daily ET results from Gibson et al. (2011).</i>	<i>28</i>
<i>Figure 4.7: Sensible heat flux calculated using TERRA and AQUA data on the same day plotted against T_0-T_a.</i>	<i>31</i>
<i>Figure 4.8: Dependence of roughness length and displacement height on height and density of roughness elements (e.g. trees) (Kipp & Zonen, 2005).....</i>	<i>32</i>
<i>Figure 4.9: The process of allocating z_0 and d_0 values in the P10A catchment. A. Modified landcover map, B. Landcover by MODIS pixel, C. Allocated roughness lengths and D. Displacement heights.....</i>	<i>36</i>
<i>Figure 4.10: Summer scene, P10A, DOY 017: Sensitivity of sensible heat flux to z_{0m} and T_0-T_a.</i>	<i>37</i>
<i>Figure 4.11: Winter scene, P10A, DOY 217: Sensitivity of sensible heat flux to z_{0m} and T_0-T_a.</i>	<i>37</i>
<i>Figure 4.12: Winter scene, P10A, DOY 185: Sensitivity of sensible heat flux to z_{0m} and T_0-T_a.</i>	<i>38</i>
<i>Figure 4.13: Catchment average ET calculated for G30G using the SEBS model with AQUA and TERRA data and plotted against ET_0.....</i>	<i>39</i>
<i>Figure 4.14: Catchment average ET calculated for P10A using the SEBS model with AQUA and TERRA data and plotted against ET_0.....</i>	<i>39</i>
<i>Figure 4.15: AQUA SEBS ET results for each date processed for the G30G catchment plotted against T_0-T_a</i>	<i>40</i>
<i>Figure 4.16: AQUA SEBS ET results for each date processed for the P10A catchment plotted against T_0-T_a</i>	<i>40</i>
<i>Figure 4.17: AQUA SEBS evaporative fraction results for each date processed for the G30G catchment plotted against T_0-T_a</i>	<i>42</i>

<i>Figure 4.18: AQUA SEBS evaporative fraction results for each date processed for the P10A catchment plotted against T_0-T_a.....</i>	<i>42</i>
<i>Figure 4.19: Catchment average daily ET for G30G from the ET-API method compared with ET_0 from the Sandberg weather station for the study period (July 2006-June 2007)43</i>	
<i>Figure 4.20: Catchment average daily ET for P10A from the ET-API method compared with ET_0 from the Rockhurst weather station</i>	<i>44</i>
<i>Figure 5.1: Rain gauges used to validate ARC-ISCW grid results for G30G (A) and P10A (B).....</i>	<i>46</i>
<i>Figure 5.2: ARC-ISCW grid values against rainfall measured at the validating stations in G30G for study period totals (on the left) and monthly values (on the right)</i>	<i>46</i>
<i>Figure 5.3: ARC-ISCW grid values against rainfall measured at the validating stations in P10A for study period totals (on the left) and monthly values (on the right)</i>	<i>47</i>
<i>Figure 6.1: Geology of G30G catchment and surrounds</i>	<i>50</i>
<i>Figure 6.2: Groundwater levels in G30G versus ARC-ISCW catchment average rainfall51</i>	
<i>Figure 6.3: Geological map of P10A and surrounds also showing borehole locations ..</i>	<i>52</i>
<i>Figure 7.1: SHARE soil moisture data plotted against rainfall for G30G (A) and P10A (B).....</i>	<i>55</i>
<i>Figure 7.2: SHARE soil moisture data plotted against ET_0 for G30G (A) and P10A (B).....</i>	<i>56</i>
<i>Figure 7.3: Median soil moisture values in G30G.</i>	<i>57</i>
<i>Figure 7.4: Median soil moisture values in P10A.</i>	<i>57</i>
<i>Figure 8.1: G30G runoff at G3H001 Tweekuilen versus rainfall</i>	<i>59</i>
<i>Figure 8.2: P10A runoff at P1H003 Boesmansrivier versus rainfall</i>	<i>60</i>
<i>Figure 9.1: G30G water balance</i>	<i>61</i>
<i>Figure 9.2: G30G cumulative rainfall, ET-API and ET_0.....</i>	<i>63</i>
<i>Figure 9.3: P10A water balance</i>	<i>64</i>
<i>Figure 9.4: P10A cumulative rainfall, ET-API and ET_0.....</i>	<i>65</i>
<i>Figure A1: Map of sites to visit for field sampling of ET</i>	<i>74</i>
<i>Figure A2: Northern part of study area looking south from sample point 14</i>	<i>75</i>
<i>Figure A3: Southern part of study area, more thickly vegetated.....</i>	<i>75</i>
<i>Figure A4: The ARC-API Grahamstown team, GEOSS, SU and ARC-ISCW</i>	<i>77</i>
<i>Figure A5: SEBS parameters checked during field visit</i>	<i>83</i>

List of Tables

<i>Table 2.1: Total area per catchment of percentage of landcover class per MODIS pixel showing homogeneity and heterogeneity per catchment</i>	<i>10</i>
<i>Table 3.1: Landcover classes for the G30G quaternary catchment</i>	<i>12</i>
<i>Table 3.2: Landcover classes for the P10A quaternary catchment</i>	<i>14</i>
<i>Table 5.1: r^2 values showing goodness of fit between weather station data and ARC-ISCW grid results for G30G.....</i>	<i>47</i>
<i>Table 5.2: r^2 values showing goodness of fit between weather station data and ARC-ISCW grid results for P10A</i>	<i>47</i>
<i>Table 6.1: Lithostratigraphy of catchment P10A</i>	<i>52</i>
<i>Table A1: Landcover types according to NLC 2000 dataset for field sampling sites</i>	<i>76</i>
<i>Table A2: Photos, data and local knowledge per field sampling site.....</i>	<i>77</i>
<i>Table A3: Hydrocensus results – quaternary catchment P10</i>	<i>84</i>

Acronyms/Abbreviations

ARC	Agricultural Research Council
ARC-ISCW	Agricultural Research Council – Institute for Soil, Climate and Water
ASTER	Advanced Spaceborne Thermal Emission and Reflection Radiometer
BRDF	Bidirectional reflectance distribution function
d₀	Displacement height
DOY	Day of year
DWA	Department of Water Affairs
DWAF	Department of Water Affairs and Forestry
λE	Latent heat flux
ESA	European Space Agency
ET	Evapotranspiration
fc	Fractional vegetation cover
G₀	Soil heat flux
GIS	Geographical Information System
H	Sensible heat flux
H_{dry}	Sensible heat flux at dry limit
H_{wet}	Sensible heat flux at wet limit
ILWIS	Integrated Land and Water Information System
LAI	Leaf area index
MCD 43	MODIS Surface Reflectance BRDF/Albedo Product
MODIS	Moderate Resolution Imaging Spectroradiometer
NDVI	Normalized Difference Vegetation Index
NGA	National Groundwater Archive

P	Precipitation
R_n	Net radiation
RO	Runoff
SAWS	South African Weather Services
SADC	Southern African Development Community
SAR	Synthetic Aperture Radar
SEBAL	Surface Energy Balance Algorithm for Land
SEBS	Surface Energy Balance System
SMAC	Simplified method for atmospheric correction
SPOT	Système Pour l'Observation de la Terre
T_a	Air temperature
T₀	Land surface temperature
TOA	Top of atmosphere
WetSpass	Water and Energy Transfer between Soil, Plants and Atmosphere under quasi Steady State
WRC	Water Research Commission
z₀	Roughness length

Acknowledgments

- The Water Research Commission for supporting and funding this consultancy project and report.
- Dr Tony Palmer and Ms Andiswa Finca of ARC-Animal Production Institute in Grahamstown for supplying *ET* results for G30G and P10A catchment and for their contributions to the field work in the P10A catchment.
- South African Weather Service for supplying data from the Grahamstown automatic weather station.
- Mr Geoff Brown from Brakkloof Farm for borehole and rainfall records.
- Mr Mike Palmer from Strowan Farm for rainfall records.
- Dr Thomas Fyfield from ARC-ISCW for editing the report.

Chapter 1 – Introduction

This report is a follow up to WRC Report 1690/1/09 (Gibson *et al.*, 2009) entitled "Remote sensing as a tool for resource assessment towards the determination of the legal compliance of surface and groundwater use". WRC Report 1690/1/09 details a methodology to calculate water use in a catchment using remote sensing techniques as far as possible. The general approach was to use a simplified water balance where each component of the water balance equation was calculated on a grid basis using remote sensing techniques as far as possible. Methods included soil moisture estimation using radar remote sensing data, precipitation estimation from a combination of satellite imagery and interpolated rainfall from automatic weather stations, evapotranspiration (ET^1) estimation using the Surface Energy Balance System (SEBS) model (Su, 2002), runoff and recharge estimation using the Water and Energy Transfer between Soil, Plants and Atmosphere under quasi Steady State (WetSpass) model (Batelaan & De Smedt, 2001).

The results in WRC Report 1690/1/09 (Gibson *et al.*, 2009) showed that using this particular methodology, it was not possible to determine the actual water consumption of individual farms or compliance to legislation due to many uncertainties and limitations with both the input data and methodology. In this project, the aim was to address the uncertainties and limitations in WRC Report 1690/1/09 and thereby determine the efficacy or inefficiency of the method to highlight water-stressed catchments.

Perhaps the most surprising result in Gibson *et al.* (2009) was in the estimated catchment ET from the SEBS model for the study period (a hydrological year) which was nearly twice the estimated rainfall for the same catchment for the same period. This assumed overestimation of SEBS estimated ET was further highlighted when the results of an alternative model (WetSpass) were analyzed. In the SEBS model, the amount of ET is constrained by the available energy with available moisture being inferred from parameters such as vegetation cover and the differences between the land surface and air temperature. The ET estimated by the WetSpass model is

¹ In this report ET refers to actual evapotranspiration, ET_0 refers to reference evaporation as calculated from meteorological data and represents the atmospheric evaporative demand

constrained by the amount of precipitation which fell in the catchment and since it is based on a water balance, the amount of *ET* may not exceed the amount of precipitation. Interestingly, the results of both methods across a hydrological year in the Gibson *et al.* (2009) study reflected the constraining factor of their approaches respectively. Using the WetSpass model resulted in higher estimated *E_t* in the winter months where there was high water availability and using the SEBS model resulted in higher *ET* in the summer months when there is high energy availability. Although it may be possible for annual *ET* to exceed annual precipitation in certain instances, such as where large-scale irrigation from upstream or groundwater resources is practised, it is believed that *ET* was overestimated as evidence pointed towards there being limited water availability during the hot, dry summer months. Since irrigated agriculture formed a small portion of the catchment (2.4%) in comparison to natural vegetation (29.7%) and dryland agricultural (66.5%), the higher *ET* than precipitation at catchment scale could not be ascribed to evaporative losses due to irrigation.

The SEBS model is available as part of the open-source freeware ILWIS² therefore it can be used by practitioners with remote sensing knowledge who may not necessarily have the micrometeorological expertise to develop a model themselves to estimate *ET*. Whilst the open-source format of SEBS is very useful and can speed up the research process, there are some instances where specialist knowledge is required to implement the model correctly to derive the most accurate results. For this reason, the bulk of the research effort in this project has been on the *ET* component using the SEBS model. The derivation of *ET* using the SEBS model is a complex process requiring several sources of input data and numerous processing steps to derive intermediate output products. The intermediate products are then combined through additional processing algorithms to derive the final daily *ET* product. In this research we report on the potential sources of error in the operating of the SEBS model, we illustrate the propagation of these errors through the model and make recommendations regarding the choice of input data and formulae, and finally we modify the methodology used in Gibson *et al.* (2009) to minimize the sources of error which were highlighted.

² The Integrated Land and Water Information System is a free open-source GIS & Remote Sensing software, developed by ITC and available at www.52north.org

Two quaternary catchments with different hydrological regimes were selected on the basis of the availability of data (satellite, hydrological and meteorological) and the characteristics of the landscape in order to avoid complex heterogeneous situations where landuse changes over a short space and the weather conditions may vary significantly over a short distance. The selection of catchments with different hydrological regimes is to test the *ET* methodology which is based on the energy balance, in two different scenarios in summer – one where water availability is limited but energy is not and one where water availability is less of a constraint in times where energy is not a limiting factor.

The selection of the study area forms an essential and first step in this research; however, the aim was to select catchments in areas where other remote sensing *ET* research has occurred which can be used not to validate the results of the SEBS model but rather as benchmarks.

Aims

1: Study area selection

Select two quaternary catchments with different hydrological regimes which fulfill the criteria in the following importance ranking:

1. Availability of results from other remote sensing *ET* projects to benchmark *ET* results.
2. Non-complex, homogeneous landscapes with limited topographic variation
3. Reliable, historic weather station data corresponding to satellite image acquisition period.
4. Other hydrological data (e.g. water levels and river gauges)

2: Catchment *ET* using SEBS

1. Identify sources of uncertainties in the input data
2. Demonstrate the effect of these uncertainties on the results
3. Modify the method accordingly
4. Estimate daily *ET* and upscale to annual *ET*.
5. Compare the SEBS *ET* results to results from other remote sensing *ET* models.

3: Catchment precipitation using ARC-ISCW decadal rainfall grids

1. Sum monthly and annual precipitation for each catchment using individual decadal grids.
2. Obtain data from ARC-ISCW, SAWS and private weather stations which were not used in the creation of the ARC-ISCW grid.
3. Validate the accuracy of the ARC-ISCW grid using this additional rainfall data.

4: Groundwater recharge

To demonstrate groundwater recharge using water levels in support of precipitation and *ET* results.

5: Soil moisture

To use SHARE soil moisture data in support of precipitation and *ET* results.

6: Water balance

To assess the interactions between the water balance components at catchment scale by evaluating time series results of *ET* and precipitation against soil moisture, measured runoff (river gauge) and groundwater levels.

Technology transfer

The research from this project and the previous WRC Report 1690/1/09 has been well disseminated through publications. These are listed below:

Gibson L.A., Münch Z. & Engelbrecht J. 2011. Particular uncertainties encountered in using a pre-packaged SEBS model to derive evapotranspiration in a heterogeneous study area in South Africa. Hydrology and Earth System Sciences 15, 295-310.

Gibson L.A., Münch Z., Engelbrecht J. & Conrad J. 2010. Limiting uncertainties in SEBS estimated evapotranspiration in heterogeneous catchments. Presented at 2nd SAEON Summit, 5-6 October 2010, Kirstenbosch, Cape Town.

Gibson L.A., Münch Z., Engelbrecht J. & Conrad J. 2010. Uncertainties in using remote sensing for water use determination: a case study in a heterogeneous study area in South Africa. Hydrology and Earth System Sciences Discussion, 7, 6581-6612.

Gibson L.A., Münch Z., Engelbrecht J. & Conrad J. 2009. Uncertainties in using remote sensing for water use determination: a case study in a heterogeneous study area in South Africa. Presented at ESA conference on Earth Observation and Water Cycle Science, 18-20 November 2009, Frascati, Italy.

In addition, Gibson and Münch have submitted an abstract which has been accepted for presentation at the AfricaGEO conference to be hosted in Cape Town in May 2011. The title of this paper is: *“The importance of selecting accurate vegetation parameters when estimating evapotranspiration using the SEBS model – an example from a sparsely vegetated catchment, Eastern Cape”*.

Report format

We will first report on the catchment selection process (Chapter 2) which will be followed by descriptions of the selected catchments (Chapter 3). Each water balance component will then be discussed with the rationale, methodology, results and validation (where applicable) for each catchment being presented under each individual component (Chapter 4 – ET, Chapter 5 – Precipitation, Chapter 6 – Groundwater, Chapter 7 – Soil moisture and Chapter 8 – Runoff). The results of each water balance component will be combined in a time series for each catchment to analyze the interaction between each component over time (Chapter 9). Finally, conclusions regarding the efficacy or inefficacy of the method and recommendations for further research will be presented in the final chapter (Chapter 10).

Chapter 2 – Study area selection

The aim of the catchment selection process was to identify two quaternary catchments with different hydrological regimes that have satellite, hydrological and meteorological data available for input to the water balance model. Since an important part of this project is calculating *ET* using the SEBS model, validation data for *ET* would be required. This meant that the availability of *ET* validation data became the important selection criterion in identifying regions of interest.

Availability of results from other remote sensing evapotranspiration projects

At project inception, the Department of Agriculture were testing the SEBAL model in the Sandveld area, a winter rainfall region where water availability is a constraint in times where energy is not a limiting factor. The G30 tertiary catchment has been the subject of various investigations in a water scarce environment dominated by groundwater use (GEOSS, 2006). The study period was therefore selected to coincide with the availability of SEBAL validation data (July 2006 to June 2007).

Another spatial *ET* validation method has been developed by Dr Anthony Palmer of ARC-API, based on *LAI*, which has been used with good success in many areas in South Africa. This methodology that will be referred to in the text as the ET-API method is a parsimonious approach which uses the MODIS leaf area index (*LAI*) to parameterize the Penman Monteith equation (ET_{PM}) using the function:

$$ET = \frac{LAI}{LAI_{max}} \times 0.65 \times ET_{PM} \quad (1)$$

where LAI_{max} is the maximum *LAI* retrieved at the site over 10 consecutive years of MODIS data, and 0.65 is an optimized scaling factor which relates leaf-level conductance to canopy conductance (Palmer & Weideman, 2011).

A number of catchments suggested by Dr Palmer were selected for a potential area where water availability would be less of a constraint in times where energy is not a limiting factor. The study period was chosen to coincide with the period for the G30 catchments.

Figure 2.1 shows the initial selection of quaternary catchments for each hydrological regime, with all quaternary catchments from the G30 tertiary catchment selected from a winter rainfall region and the following quaternary catchments (P10A, Q91C, Q94A, R10G, R20A, R20G, S10A, S10B, S10E, S20C, S50B and S60E) selected from all year and late summer rainfall regimes.

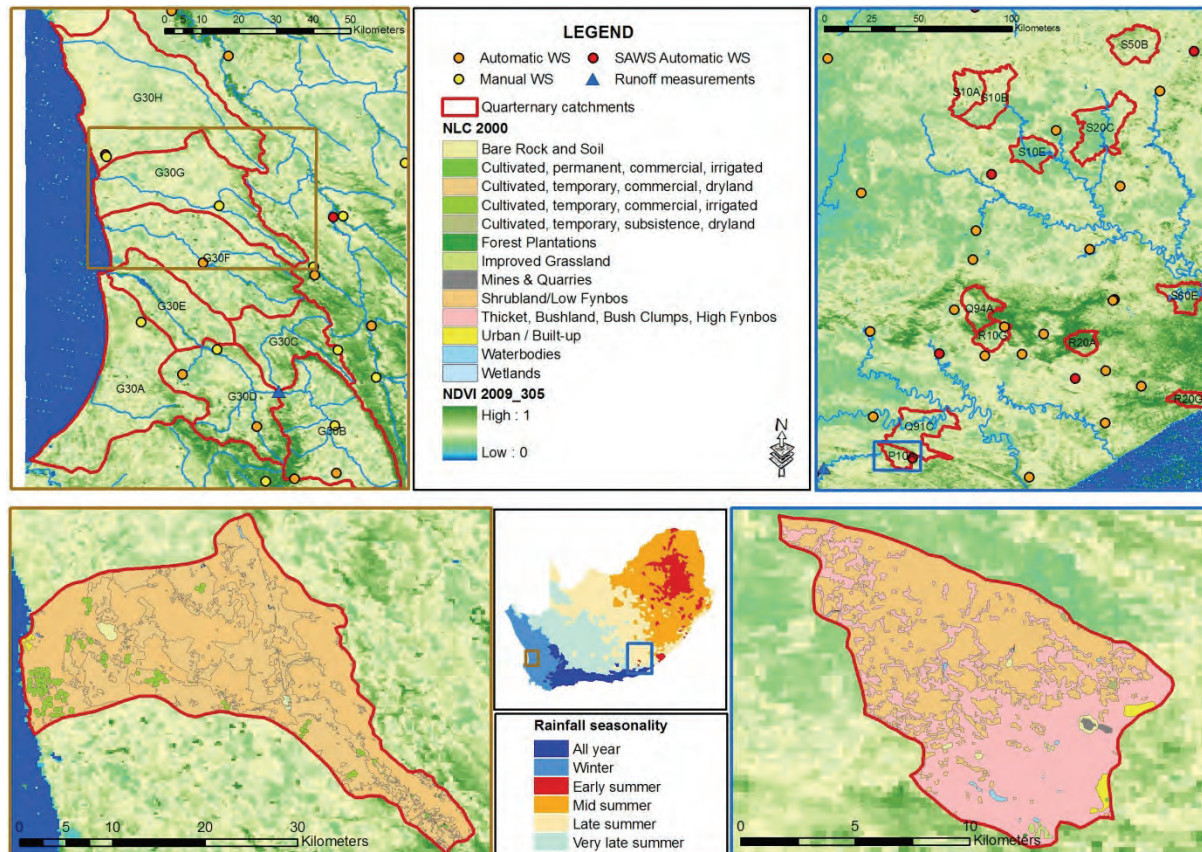


Figure 2.1: Selection of quaternary catchments for each hydrological regime

Non-complex, homogeneous landscapes with limited topographic variation

According to Gibson *et al.* (2009), heterogeneity of the study area plays an important role in creating uncertainty in *ET* results, especially where meteorological parameters are concerned. Therefore the selected catchments need to be homogeneous with little topographic variation to accommodate the fact that weather conditions may vary significantly over a short distance in a topographically complex landscape. Kustas *et al.* (2004) and Li *et al.* (2006) found that when the spatial resolution exceeds 500 m, mixed pixels containing large contrasts in surface temperature and vegetation cover could cause significant errors (Li *et al.*, 2008). Flores *et al.*

(2009) demonstrated the impact of topographic heterogeneity on near-surface soil temperature and McCabe & Wood (2006) found that although MODIS has limited capacity in capturing the spatial variability in fluxes at field level, estimates for the spatial average flux at large scales may be accurate. Gibson *et al.* (2011) also found that although the proportional partitioning of energy compared well between lower resolution (MODIS) and higher resolution (ASTER) results, the upscaling of evaporative fraction to daily *ET* differed at varying resolutions.

Heterogeneity of the study area was firstly investigated by looking at the landcover distribution within the 1000 m MODIS pixel. The area (ha) of a particular landcover class was expressed as a percentage of the total area per MODIS pixel. Figure 2.2 gives the results for G30G (A) and P10A (B).

For each catchment, the area where 80-100% and 90-100% of a MODIS pixel was consumed by a particular landcover class was summed and expressed as a percentage of the total area for the catchment. Similarly the area where less than 20% of a MODIS pixel was covered by a particular landcover class was also calculated as a percentage of total catchment area. Table 2.1 gives the results for each catchment of the highest percentage landcover homogeneity and heterogeneity.

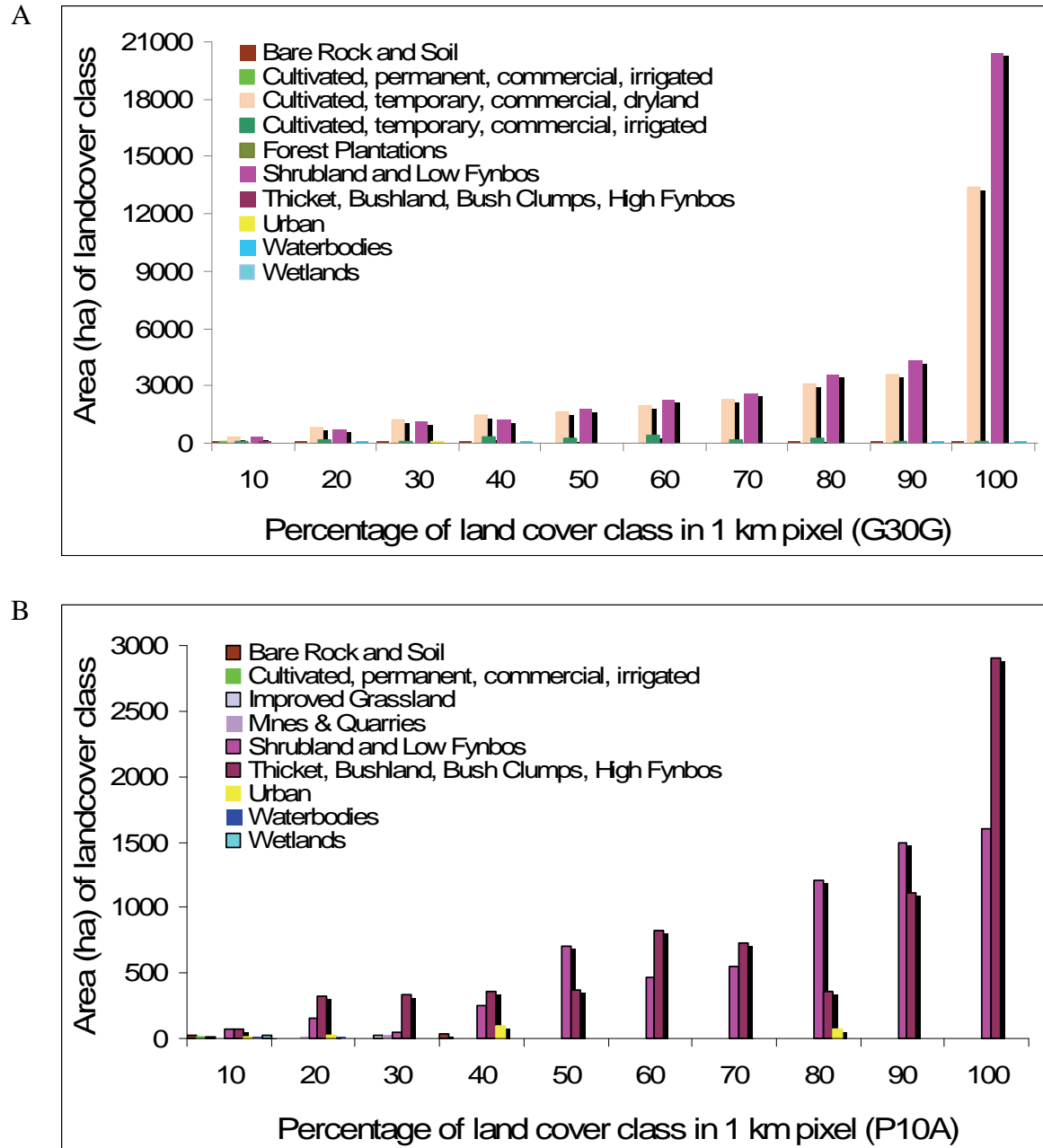


Figure 2.2: Percentage of landcover class per MODIS pixel in G30G (A) and P10A (B)

From Table 2.1, G30F, G30G and G30H, as well as P10A, R10G and Q94A were selected for further investigation and finally only G30F and G30G, as well as P10A and R10G were shortlisted for selection based on a similar exercise, this time at a scale of 250 m. These catchments were then further compared based on topography and NDVI. The final selection per catchment was based on the availability of additional data sources and specifically available weather data.

Table 2.1: Total area per catchment of percentage of landcover class per MODIS pixel showing homogeneity and heterogeneity per catchment

% of landcover class per pixel	Area per catchment		
	%90-100	%80-100	%0-20
G30A	38.4	51.4	5.5
G30B	55.0	64.7	5.3
G30C	18.8	30.6	8.1
G30D	33.0	45.4	6.6
G30E	44.4	56.3	5.5
G30F	40.3	51.9	5.2
G30G	47.6	59.0	4.0
G30H	60.3	70.4	2.8
P10A	31.4	49.5	5.6
Q91C	19.0	35.8	5.1
Q94A	36.3	43.8	10.4
R10G	55.9	66.3	5.2
R20A	19.5	30.2	12.8
R20G	22.2	35.0	14.6
S10A	11.2	26.5	6.1
S10B	20.9	41.3	10.8
S10E	8.6	20.0	13.4
S20C	22.7	32.5	10.3
S50B	23.4	39.6	12.1
S60E	19.8	38.5	5.7

Reliable, historic weather station data corresponding to satellite image acquisition

G30G and P10A were finally selected as the most suitable catchments. Historic weather station data from automatic weather stations (AWS) (ARC-ISCW Sandberg for G30G and ARC-ISCW Rockhurst and SAWS Grahamstown for P10A) were used as input to the SEBS model for calculating ET. For the demonstration of the water balance, decadal rainfall grids were obtained from ARC-ISCW. These were aggregated to monthly rainfall grids and validated against weather stations within the study areas.

Other hydrological data (e.g. water levels and river gauges)

Hydrological river gauge data were obtained from DWAF. The selected catchments did not feature a river gauging station, but information was taken from an upstream gauge (G3H001) for G30G and a downstream gauge (P1H003) for P10A. Groundwater level data were obtained from DWAF NGA.

Chapter 3 – Study area description

G30G

Quaternary catchment G30G (647 km² in area) is located in the northern Sandveld about 300 km north of Cape Town. It has an elongated curved shape and originates in the quartzitic mountains of the Langberg and Uitkomsberge with an altitude of 813 m and 672 m above mean sea level respectively. The upper reaches of the catchment comprise mountainous and rugged terrain. At the mid-point of the catchment the topography changes and is much flatter with subdued topographical variation. The transition from mountainous area to flatter-lying, sand-covered topography occurs at an elevation of approximately 200 mamsl.

The Jakkals River drains the catchment and flows into the Jakkalsvlei at Lamberts Bay. The only other town within the catchment is Graafwater located close to the mid-point. As the catchment is within an arid environment the river flow is highly seasonal. The Jakkals River is a small, mostly non-perennial river system and only flows in winter. In summer the stagnant pools are the only evidence of a river system and the mean annual runoff is 5.4 mm/a. Groundwater is the domestic water source for the towns with the town of Graafwater consuming 15 840 kl/m of groundwater in summer and 7 540 kl/m in winter in 2005.

The catchment contains large agricultural areas. It is estimated that in 2004 the agricultural sector abstracted 1.642 Mm³ for irrigation – mainly potatoes. Up until 2004 the total area cleared for growing potatoes was 2 556 ha, with 238 ha actually planted. Approximately 21% of the groundwater recharge (8.28 Mm³/a) was abstracted by the agricultural and municipal sectors in 2004 (GEOSS, 2006).

The landcover types which constitute the quaternary catchment of G30G are listed in Table 3.1.

Table 3.1: Landcover classes for the G30G quaternary catchment

Landcover	% of Total Area
Bare Rock and Soil (erosion: sheet)	0.02
Bare Rock and Soil (natural)	0.63
Cultivated, permanent, commercial, irrigated	0.12
Cultivated, temporary, commercial, dryland	41.37
Cultivated, temporary, commercial, irrigated	3.09
Forest Plantations (Other / mixed spp)	0.06
Shrubland and Low Fynbos	54.10
Thicket, Bushland, Bush Clumps, High Fynbos	0.13
Urban / Built-up (residential)	0.20
Urban / Built-up (residential, formal suburbs)	0.07
Urban / Built-up (residential, formal township)	0.04
Urban / Built-up, (commercial, mercantile)	0.03
Waterbodies	0.09
Wetlands	0.05

Catchment G30G falls within a winter rainfall region and receives approximately 253 mm/a (Middleton & Bailey, 2008). Low rainfall is experienced along the coast and extending inland for a short distance, thereafter increasing as topography increases. The lowest rainfall (~1 mm/month) is experienced in January and the highest (varying from 30 mm at the coast to 89 mm at the most southern portion of the catchment) in June. The average midday temperature is 18°C in July which is the coldest month, with night time temperatures dropping to an average of 6-7°C. February is the hottest month with average midday highs of 29°C at Lamberts Bay and 31°C at Graafwater. Inter-annual climatic variability is reported for the G30G catchment (GEOSS, 2006).

The vegetation types within the catchment comprise mostly Leipoldtville Sand Fynbos (50.4%), followed by Lamberts Bay Strandveld (26%) and Graafwater Sandstone Fynbos (20.6%). Other vegetation types include Cape Seashore Vegetation, Cape Estuarine Salt Marshes and Cederberg Sandstone Fynbos (Mucina & Rutherford, 2004).

P10A

Quaternary catchment P10A is located immediately to the north-west of Grahamstown. It is a 'pear shaped' catchment with a total area of 125.6 km². It comprises undulating topography with valleys that are quite deeply incised in places. The topographical elevation in the catchment ranges from 487 mamsl to 806 mamsl. The annual average rainfall is 466 mm/a. The rainfall in the area is lowest in the cold winter months of June and July. It receives the lowest rainfall (~16 mm/month) in July and the highest (~57 mm/month) in March (October is also a high rainfall month). The monthly distribution of average daily maximum temperatures shows that the average midday temperatures for Grahamstown range from 18.9°C in July to 26.8°C in February. The region is the coldest during July when the temperature drops to 5.6°C on average during the night.

The main river draining the catchment is the New Years River, a tributary of the Boesmans River. It flows in a north-westerly direction and exits the catchment to the west. The New Years River is un-gauged and there are numerous storage dams within the catchment.

The landcover which most commonly occurs in catchment P10A, is 'Thicket, Bushland, Bush Clumps, High Fynbos' (Table 3.2). The next most commonly occurring landcover class is "Shrubland and Low Fynbos". These two classes make up 97.2 % of the entire catchment. There are 13 landcover classes within the catchment.

The rainfall distribution across quaternary catchment P10A has a clear trend. The highest rainfall occurs in the southern portion of the catchment (~800 mm/a). The rainfall reduces steadily northwards with the lowest rainfall occurring in the northern portion of the catchment (~451-490 mm/a). This rainfall gradient is steep as the lowest rainfall is approximately half the volume of the highest rainfall. The annual A-pan evaporation for the catchment also shows a clear trend; however, the lowest evaporation occurs in the southern portion of the catchment (~1750 mm/a) and increase northwards (~1900 mm/a).

Table 3.2: Landcover classes for the P10A quaternary catchment

Landcover type	% of Total Area
Bare Rock and Soil (erosion: dongas / gullies)	0.5
Cultivated, permanent, commercial, irrigated	0.04
Cultivated, temporary, subsistence, dryland	0.2
Forest Plantations (Eucalyptus spp)	0.02
Improved Grassland	0.3
Mines & Quarries (surface-based mining)	0.3
Shrubland and Low Fynbos	47.9
Thicket, Bushland, Bush Clumps, High Fynbos	49.3
Urban / Built-up (rural cluster)	0.5
Urban / Built-up (smallholdings, shrubland)	0.06
Urban / Built-up, (industrial / transport: heavy)	0.5
Waterbodies	0.3
Wetlands	0.2

The most commonly occurring vegetation types within the catchment are Bhisho Thornveld (75.2 %) and Suurberg Quartzite Fynbos (21.4%). A very small portion of the catchment comprises Albany Broken Veld and Suurberg Shale Fynbos (Mucina & Rutherford (2004).

Chapter 4 – Evapotranspiration

Remote sensing energy balance methods use empirical relationships and physical modules from remotely sensed and meteorological data. The Surface Energy Balance Index (SEBI) model was the foundation for the remote sensing based surface energy balance approach (Badola, 2009). This approach is based on a complete simplified energy balance for each pixel where ET is predicted from the residual amount of energy remaining from the classical energy balance equation.

$$\lambda E = R_n - G_0 - H \quad (2)$$

where λE is the turbulent latent heat flux (λ is the latent heat of vaporization and E is water vapour flux density), R_n is net radiation, G_0 is the soil heat flux and H is the sensible heat flux (Su, 2002).

Models such as Surface Energy Balance Algorithm over Land (SEBAL) (Bastiaanssen *et al.*, 1998), and SEBS (Su, 2002) use remote sensing directly to estimate input parameters and ET . Badola (2009) points out that each algorithm developed for energy balance closure over land has its own advantages and disadvantages. The SEBAL model, which is probably the widest published remote sensing ET model, is designed for regional ET calculations. SEBAL uses surface temperature, surface reflectance and NDVI together with their interrelationships to deduce surface fluxes (Bastiaanssen *et al.*, 1998). Threshold values are extracted from wet and dry surfaces on the studied area. The sensible heat flux is computed by inverting the sensible heat flux expression over both dry ($\lambda E = 0$) and wet ($H = 0$) land with latent heat flux being computed as the residual of the energy balance. The major advantage of SEBAL is that it demands few input variables but it can only be applied to areas which have both wet- and dryland pixels available (Bastiaansen *et al.*, 1998). SEBAL is protected by intellectual property and may not be used without the developer's permission.

In contrast to SEBAL, SEBS is available as part of the free open-source software ILWIS. SEBS is a scale independent model proposed by Su (2002) for the estimation of atmospheric turbulent

fluxes and evaporative fraction using satellite earth observation data, in combination with meteorological information. Reflectance and radiance measured by the satellite are used to calculate land surface parameters – albedo, emissivity, surface temperature, fractional vegetation cover and leaf area index. Other inputs are temperature, air pressure, humidity and wind speed at reference height which are obtained from a weather station. The third input is the radiation component which can be measured directly or can be modelled. According to Su (2006), it is possible to estimate the latent heat flux as a residual after the sensible heat flux has been derived. However, because the sensible heat flux is not constrained by the available energy but is determined solely by surface temperature and the meteorological conditions at the reference height, there is an associated uncertainty in the derived latent heat flux and therefore also in the evaporative fraction. However, in SEBS this uncertainty is limited by considering the energy balance at the limiting cases. The actual sensible heat flux is constrained to the range set by the sensible heat flux at the wet limit (derived from a combination equation), and the sensible heat flux at the dry limit (set by the available energy). In SEBS, the daily *ET* is determined from the total daily available energy by assuming the evaporative fraction is constant throughout the day.

At the wet and dry limits, the equation used to calculate the sensible heat flux (Eq 3 & 4 respectively) differ from the sensible heat flux equations which are used when the wet or dry limit has not been reached (Eqs 5, 6 & 7) (Su, 2002).

$$H_{wet} = \frac{\left((R_n - G_0) - \frac{\rho C_p}{r_{ew}} \cdot \frac{e_s - e}{\gamma} \right)}{\left(1 + \frac{\Delta}{\gamma} \right)} \quad (3)$$

where e and e_s are actual and saturation vapour pressure respectively; γ is the psychrometric constant, r_{ew} is the external resistance at the wet limit and Δ is the rate of change of saturation vapour pressure with temperature.

$$H_{dry} = R_n - G_0 \quad (4)$$

$$u = \frac{u_*}{k} \left[\ln \left(\frac{z - d_0}{z_{0m}} \right) - \Psi_m \left(\frac{z - d_0}{L} \right) + \Psi_m \left(\frac{z_{0m}}{L} \right) \right] \quad (5)$$

$$\theta_0 - \theta_a = \frac{H}{ku_* \rho C_p} \left[\ln \left(\frac{z - d_0}{z_{0h}} \right) - \Psi_h \left(\frac{z - d_0}{L} \right) + \Psi_h \left(\frac{z_{0h}}{L} \right) \right] \quad (6)$$

$$L = \frac{\rho C_p u_*^3 \theta_v}{kgH} \quad (7)$$

where z is the height above the surface, u^* is the friction velocity, $k = 0.4$ is von Karman's constant, d_0 is displacement height, z_{0m} is the roughness height for momentum transfer, θ_0 is the potential temperature at the surface, θ_a is the potential air temperature at height z , z_{0h} is the scalar height for heat transfer, Ψ_m and Ψ_h are the stability correction functions for momentum and sensible heat respectively, L is the Obukhov length, g is acceleration due to gravity and θ_v is the potential virtual temperature near the surface (Su, 2002).

If H calculated from Eqs 5-7 exceeds H_{dry} calculated from Eq 4, then the dry limit is said to have been reached and Eq 4 is used to determine H . If H_{wet} calculated from Eq 3 exceeds H calculated from Eqs 5-7, then the wet limit is said to have been reached and Eq 3 is used to determine H .

According to formulations by Su (2002), the relative evaporation is derived from the sensible heat flux and the sensible heat flux calculated at the wet and dry limits. The relative evaporation is, in turn, used together with R_n , G_0 and the latent heat flux at the wet limit to estimate the evaporative fraction (Eqs 8 & 9).

$$\Lambda_r = 1 - \frac{H - H_{wet}}{H_{dry} - H_{wet}} \quad (8)$$

where Λ_r is relative evaporation, H is the sensible heat flux and H_{wet} and H_{dry} are the sensible heat flux at the wet and dry limits respectively.

$$\Lambda = \frac{\lambda E}{R_n - G_0} = \frac{\Lambda_r \cdot \lambda E_{wet}}{R_n - G_0} \quad (9)$$

where Λ is the evaporative fraction and λE and λE_{wet} are the latent heat flux and the latent heat flux at the wet limit respectively.

In SEBS it is assumed that the daily value of evaporative fraction is approximately equal to the instantaneous value, and from this, the daily ET can be determined as:

$$ET = 8.64 \times 10^7 \times \frac{\Lambda \cdot \overline{R_n}}{\lambda \rho_w} \quad (10)$$

where ET is the actual evaporation on daily basis (mm.d^{-1}), λ is the latent heat of vaporization (J.kg^{-1}), ρ_w is the density of water (kg.m^{-3}) and $\overline{R_n}$ is the daily net radiation flux (Li *et al.*, 2008).

The daily net radiation flux is given as:

$$\overline{R_n} = (1 - c_1) \cdot r_o \cdot K \downarrow_{day} + L_{day} \quad (11)$$

where c_1 is a conversion factor of 1.1 for instantaneous to broad band albedo, r_o is broad band albedo and used in the instantaneous net radiation flux calculation in SEBS, $K \downarrow_{day}$ is incoming shortwave radiation (measured or modelled) and L_{day} is daily longwave radiation (Hailegiorgis, 2006). It can be seen from Eqs 10 & 11 that aside from evaporative fraction itself, albedo is the sole remote sensing derived variable used in the upscaling from instantaneous evaporative to daily ET .

Published results of the SEBS model have been validated with a variety of field and/or complementary methodologies such as the extremely localized lysimeter (Lin, 2006), flux tower measurements using Eddy covariance or Bowen Ratio methods (Su, 2002; Su *et al.*, 2005; Timmermans *et al.*, 2005; McCabe & Wood, 2006; Badola, 2009; Van der Kwast *et al.*, 2009),

the large aperture scintillometer (Jia *et al.*, 2003; Timmermans *et al.*, 2005). Additionally, results have been compared to hydrometeorological equations (Hailegiorgis, 2006; Lin, 2006; Gebreyesus, 2009) and the water balance or by examining hydrological consistency with other datasets (Su & Roerink, 2004; Alvarez, 2007; McCabe *et al.*, 2008; Pan *et al.*, 2008).

Several authors have addressed the sensitivity of the SEBS model to various input parameters including: roughness length (Lin, 2006; Alvarez, 2007; Van der Kwast *et al.*, 2009, Gebreyesus, 2009), displacement height (Lin, 2006), land surface temperature (Badola, 2009; Van der Kwast *et al.*, 2009), wind speed and wind direction (Van der Kwast *et al.*, 2009), fractional vegetation cover (Badola, 2009; Lin, 2006), surface emissivity (Badola, 2009; Van der Kwast *et al.*, 2009; Lin, 2006), albedo (Badola, 2009; Van der Kwast *et al.*, 2009), NDVI (Badola, 2009; Van der Kwast *et al.*, 2009), shortwave incoming radiation (Van der Kwast *et al.*, 2009) and the height of the planetary boundary layer (Van der Kwast *et al.*, 2009).

In the formulation publication of SEBS (Su, 2002), the sensitivity of the sensible heat flux to parameters³ used in its calculation was found to be around 40 W.m⁻² when the various terms are assumed independent of each other. Since in reality at least some of the terms are correlated, the expected sensitivity can then be estimated in the order of 20 (W.m⁻²), which is around 20% relative to the mean sensible heat flux (H) (Su, 2002). Of the reported sensitivities since the work of Su (2002), Badola (2009) and Van der Kwast *et al.* (2009) reported SEBS to be most sensitive to land surface temperature. However, Lin (2006) reported that the SEBS model is most sensitive to roughness length and according to Van der Kwast *et al.* (2009), sensitivity to aerodynamic parameters (roughness length, displacement height and canopy height) and the method used to derive these parameters should be considered depending on the heterogeneity of the image footprint.

The derivation of ET through the SEBS model has been shown to be a complex process requiring several sources of input data and several processing steps to derive intermediate output products. The intermediate products are then combined through additional processing algorithms to

³ land surface temperature and air temperature gradient, friction velocity, excess resistance to heat transfer, and stability correction function for heat transfer.

eventually derive the final daily *ET* product. The complexities associated with the derivation of *ET* and associated uncertainties imply that potential errors may be introduced at various stages of *ET* derivation (Gibson *et al.*, 2010).

This report aims to address uncertainties raised in the report by Gibson *et al.* (2009), and in a Hydrology and Earth System Science discussion paper by Gibson *et al.* (2010), so that the uncertainties associated with the input data are limited at MODIS resolution, and issues within the SEBS model itself are addressed. If this can be achieved, it will be possible to assess the accuracy of the SEBS model and make recommendations for its further use or required research direction before operational implementation is recommended. The ILWIS open-source freeware format of SEBS may lead to it becoming widely used in South Africa and therefore the accuracy of the model itself in the South African environment should be established as soon as possible. Furthermore, the complexity of the SEBS model together with the inherent uncertainty in using remote sensing derived products as input implies that a large number of sources of uncertainty may exist and should be properly understood.

The issues which will be dealt with in the next sections will be the effects of the atmosphere, the choice of fractional vegetation cover formula, the impact of land surface air temperature gradient and time of day at which the satellite image was captured, and finally the importance of accurate roughness length and displacement height estimates in combination with the reference height.

1: Atmospheric effects:

The accurate retrieval of surface reflectance and temperature is very important in deriving land surface biophysical parameters and in the determination of fluxes. In mapping the surface physical properties the surface information is highly affected by atmospheric components (scattering by aerosols and absorption by gases, such as oxygen, water vapour and ozone) and their magnitude (Hailegiorgis, 2006). The simplified method for atmospheric correction (SMAC) proposed by Rahman & Dedieu (1994) has been programmed into ILWIS to correct for the effects of the atmosphere on MODIS visible, near infrared and shortwave infrared data. SMAC is a radiative transfer model and therefore requires a description of the components in the atmospheric profile in order to correct for these effects.

Each of the reflective bands (bands 1-5 & 7) is atmospherically corrected using SMAC. Due to many pixels of missing data in the MODIS atmospheric products over the Gibson *et al.* (2009) study area, mean values were used to correct for the entire study area leading to some doubt as to the accuracy of the method.

Gibson *et al.* (2011) compared the results of SEBS estimated *ET* from a non-atmospherically corrected ASTER image and MODIS image with the results from the same atmospherically corrected images. When the SEBS model was run on the corrected images, it was apparent that the albedo estimation on the ASTER image in particular was unrealistically low when compared with literature values. When the albedo calculation was carried out on the ASTER image which had not been atmospherically corrected, the albedo values more closely matched literature values. This low albedo has a particular impact at the level where the instantaneous evaporative fraction is upscaled to daily *ET* and where albedo is low, a higher daily *ET* result is returned. The use of accurately atmospherically corrected images is therefore vital to mitigate the overestimation of *ET*.

To negate the need for atmospherically correcting MODIS level 1B images as was the approach of Gibson *et al.* (2009), the MCD 43 – Surface Reflectance BRDF/Albedo Product – specifically MCD43A4 can be used. The models used in creating this product best describe the differences in radiation due to the scattering (anisotropy) of each pixel and rely on multi-date, atmospherically corrected, cloud-cleared input data measured over 16-day periods. Both Terra and Aqua data are used in the generation of this product, providing the highest probability for quality input data (<http://modis-land.gsfc.nasa.gov/brdf.htm>). This corrected data can then be used for the calculation of all input parameters derived from the MODIS reflective bands on the assumption that parameters such as albedo, NDVI and fractional vegetation cover generally do not significantly change over a 16-day period. Although this assumption may not always hold true especially after rainfall events following a prolonged dry period, at an annual time scale, phenological changes are probably adequately captured.

To minimize the influence of the atmosphere on the MODIS radiative bands which are used to derive land surface temperature, the day of year which was predominantly used in each

catchment for the MCD43A4 can be considered. The MODIS data products select the best quality data in the 16-day period to estimate the reflectance products. The assumption is therefore made that on that particular day, factors such as atmospheric effects (including the presence or absence of clouds) and solar and sensor zenith angles are most favourable and the best quality thermal infrared data will also be available.

The atmospheric transmissivity on a particular day can also be considered. Atmospheric transmissivity (also known as the clearness index) is the ratio of global solar radiation at ground level to extra-terrestrial solar radiation. An example of the top of atmosphere (TOA) radiation versus the shortwave radiation which reaches the land surface is show in Figure 4.1 where it can be seen that the TOA radiation is a perfect sinusoidal curve whereas the surface shortwave radiation is erratic as it is influenced by atmospheric particles and cloud cover. The atmospheric transmissivity should be calculated at image capture time for selected images by dividing the solar radiation measured at the appropriate weather station by the calculated extra-terrestrial solar radiation from date, latitude and time of day. Images with the highest atmospheric transmissivity should be selected for further analysis.

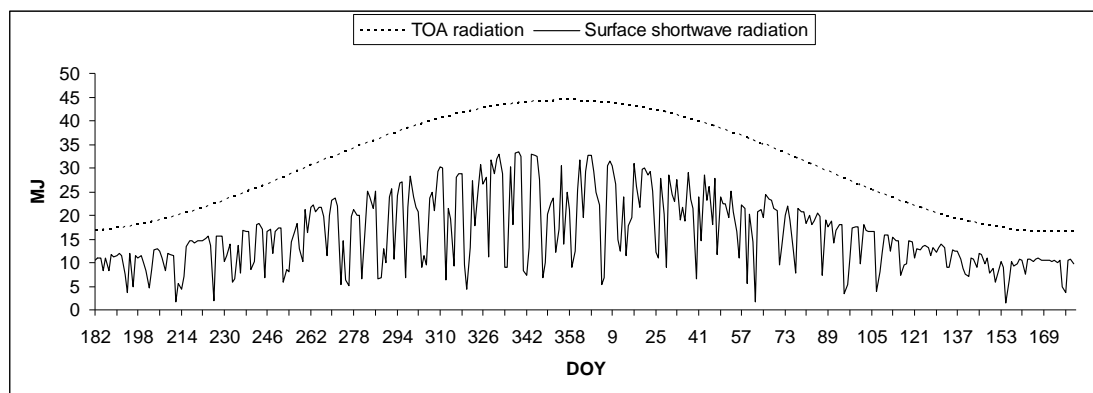


Figure 4.1: An example of top of atmosphere radiation versus surface shortwave radiation at the same location

Application to this research:

Each 16-day MCD43A4 data for the study period was selected with some images being excluded due to prolonged periods of rainfall. The date selection of thermal bands from MODIS TERRA or AQUA level 1B data within the 16-day period is done by analyzing the selected DOY most represented in each catchment from the MCD43A4 quality data. Since the MODIS Science team

selects the best quality data to include in the MODIS data product on the basis of view angles, cloud cover and atmospheric effects, the assumption is that the best quality thermal data will be captured simultaneously. Level 1B data on the selected DOY is used to calculate the land surface temperature according to the method described in Gibson *et al.* (2009) and weather station data corresponding to the date and time of day of image capture is selected.

The daily top of atmosphere radiation and atmospheric transmissivity is calculated and those image dates which have high atmospheric transmissivity are selected for further processing with the aim of selecting monthly images evenly distributed throughout the year (Figures 4.2 & 4.3). On occasion other factors such as missing weather data records can influence the final choice of image dates or the daily atmospheric transmissivity may be low. There were occasions where the daily transmissivity was low but at time of image capture the instantaneous transmissivity was acceptable. In these cases, the image can still be selected. The recommended use of transmissivity is suggested as a guideline to help in the date selection process and it should not be used as a deterministic rule.

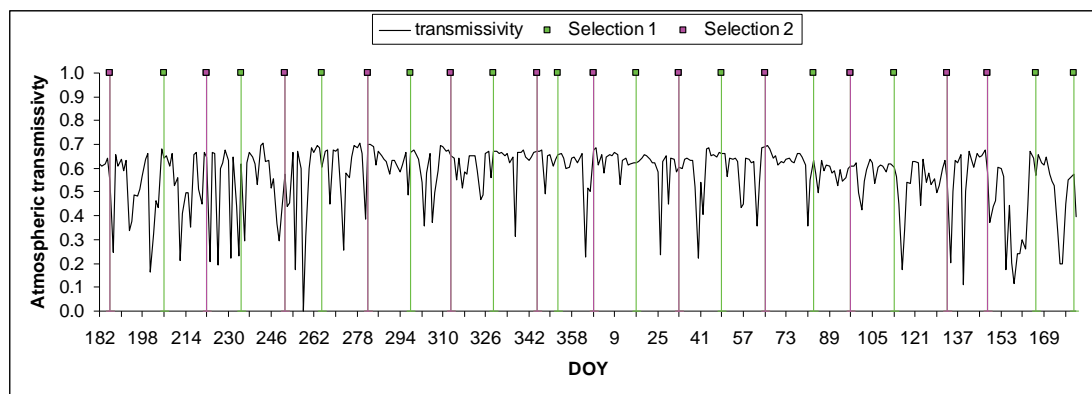


Figure 4.2: Image date selection for G30G. Selection 1 represents those dates which were selected in the first iteration but were subsequently rejected. Selection 2 represents the image DOYs which were finally chosen for further processing

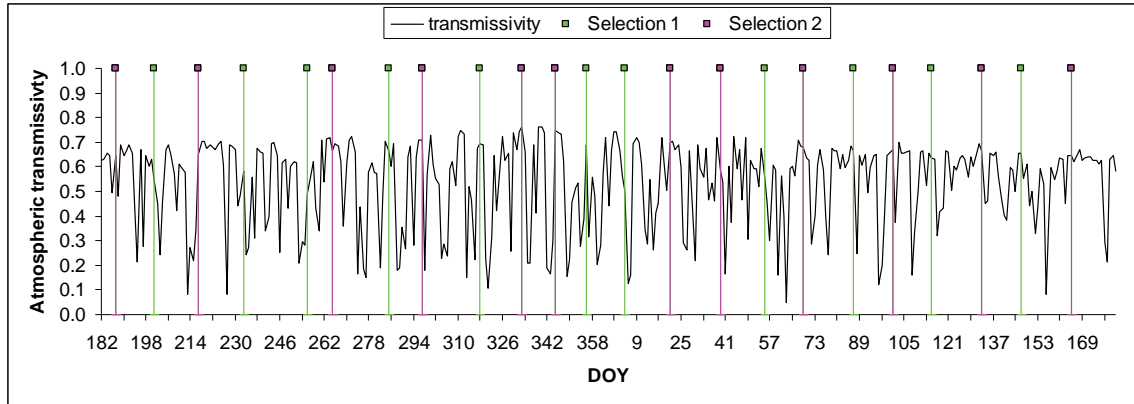


Figure 4.3: Image date selection for P10A. Selection 1 represents those dates which were selected in the first iteration but were subsequently rejected. Selection 2 represents the image DOYs which were finally chosen for further processing

A potential shortcoming of selecting those days with the greatest atmospheric transmissivity should be noted. It is possible that a bias towards days with higher *ET* is being introduced by selecting those days with highest atmospheric transmissivity and therefore those days with the most energy reaching the earth's surface.

2: Fractional vegetation cover:

Fractional vegetation cover (*fc*) is a user defined input into the pre-packaged version of SEBS in ILWIS and different formulations of *fc* are used in SEBS for different purposes. Fractional vegetation cover and its complement are used in the calculation of the roughness length for heat transfer (Su *et al.*, 2005) which, in turn, is used in the calculation of the sensible heat flux. In addition, *fc* is used in the estimation of the soil heat flux (Su, 2002) and in the preprocessing stages to assign surface emissivity values (Sobrino & El Kharraz, 2003) which are used to derive land surface temperature.

Gibson *et al.* (2011) advise that care should be taken when selecting fractional vegetation cover formula as this should be appropriate for the study area, especially if NDVI minimum and maximum values need to be defined. In particular, it is advised that if a leaf area index product is available at the appropriate scale, that it be used to estimate fractional vegetation cover according to the formula by Choudhury (1987).

Gibson *et al.* (2011) highlight that there are several methods for the calculation of f_c which are described in the literature. These methods generally make use of LAI (Choudhury, 1987) as input or require pixel NDVI together with a minimum and maximum NDVI value (Carlson & Ripley, 1997; Gutman & Ignatov, 1998). These minimum and maximum NDVI values are either constant (Sobrino & El Kharraz, 2003) or can be derived directly from the scene or from a time series. For example, if fractional vegetation cover is calculated according to the formula for vegetation proportion (Sobrino & El Kharraz, 2003), then NDVI minimum is defined to be 0.2 and NDVI maximum is 0.5, where pixels with NDVI values of 0.5 or higher are considered to be fully vegetated and pixels with values of 0.2 or lower to be bare soil. The values between NDVI minimum and maximum represent the mixed vegetation cover with differing degrees of sparse vegetation.

Gibson *et al.* (2011) concluded that if it is possible to obtain field data in order to derive an appropriate NDVI maximum value, the formula by Carlson & Ripley (1997) can be used. Alternatively the formula by Choudhury (1987) using LAI as input may be used.

Application to this research:

In this research two approaches were used to calculate fractional vegetation cover. For P10A catchment the formula by Carlson & Ripley (1997) was used with NDVI minimum and maximum values being derived from a time series analysis of NDVI values for the study area during the study period. In Figure 4.4 it can be seen that for the P10A catchment, the maximum NDVI ranged from 0.76 to 0.89. In order to exclude outliers in the maximum NDVI per scene the 98th percentile value of 0.756 was used as an NDVI maximum for the P10A catchment.

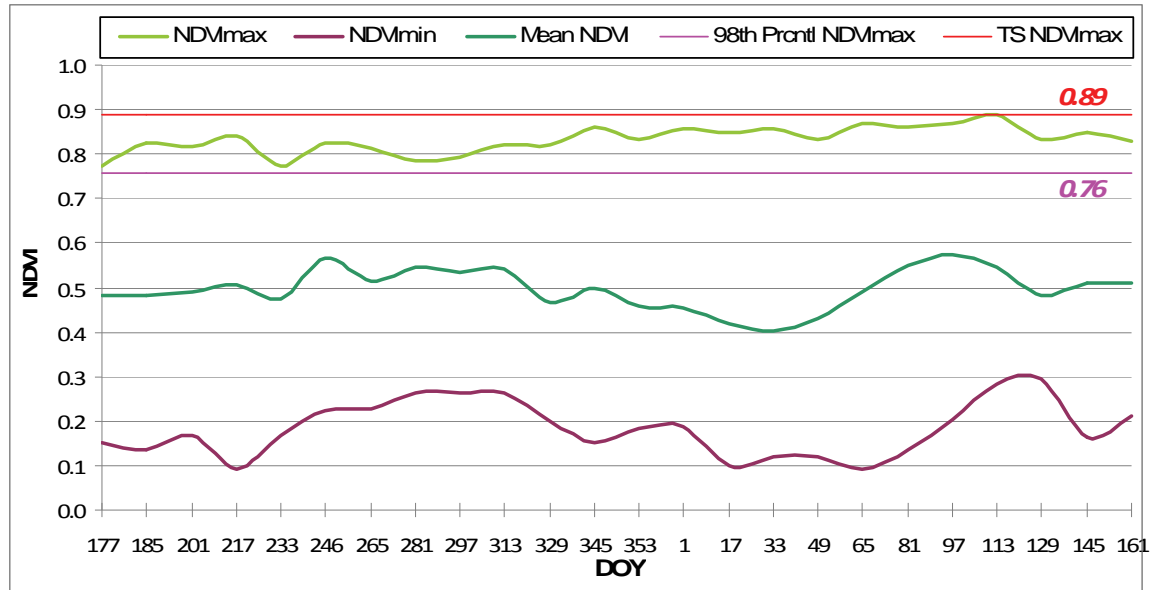


Figure 4.4: NDVI values for the P10A catchment across the study period. The 98th percentile value was used to define the NDVI maximum value in the fractional vegetation cover formula

To show an alternative approach, the MODIS LAI data product was used for the G30G catchment. The effect on the calculated sensible heat flux and the sensible heat flux at the wet and dry limits of using the two approaches is shown in Figure 4.5 where the difference in results when using the LAI approach and the NDVI maximum approach is plotted, using 8 January 2007 in G30G by way of example. It can be seen that when using the LAI approach, the calculated sensible heat flux (H) is higher by 0-20 W.m^{-2} . The calculated sensible heat flux at the dry limit (H_{dry}) is higher by 10-30 W.m^{-2} and the sensible heat flux at the wet limit (H_{wet}) is generally lower by -10 - -20 W.m^{-2} . The changes in H_{wet} and H_{dry} are due to the influence of fractional vegetation cover on the soil heat flux (G_0) alone as can be seen in Eqs 3 & 4, whereas the change in H is due to the use of fractional vegetation cover (and its complement) in the calculation of roughness length for heat transfer (Su, 2002). In this particular example, it is therefore shown that using ill-defined NDVI maximums to estimate fractional vegetation resulted in a lowering of the sensible heat flux which would contribute to overestimations of ET.

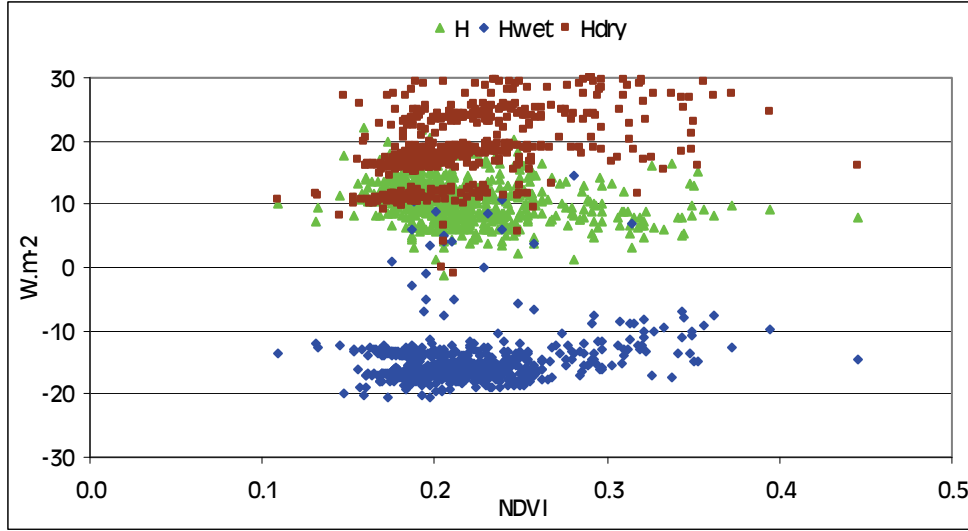


Figure 4.5: Difference in sensible heat flux results when using the LAI or NDVI approach to calculate the fractional vegetation cover. The results obtained with using the NDVI approach are subtracted from the results obtained with the LAI approach

3: Land surface and air temperature gradient

The calculation of ET using the SEBS model relies on two temperature sources: air temperature (T_a) and land surface temperature (T_0). Su (2002) reported on the sensitivity of sensible heat flux to the gradient between land surface temperature and air temperature and Badola (2009) reported that of all remotely sensed input parameters, SEBS was most sensitive to change in T_0-T_a . T_0 plays a role in the determination of net radiation and therefore soil heat flux, but its main contribution (together with the aerodynamic resistance) is in the calculation of the sensible heat flux.

It can be seen from Eqs 3 & 4 that at the wet and dry limits, the land surface and air temperature gradient is not considered in the calculation of the sensible heat flux. For this reason, T_0-T_a does not play a role in the calculation of E_{ta} if the wet or dry limits have been reached. However, T_0-T_a is used to determine whether or not the limits are reached (Eqs 5-7) and therefore should not be completely discounted in these instances.

Gibson *et al.* (2011) reported on the calculated sensitivity of the sensible heat flux $\Delta(T_0-T_a)$ for two different environments and were able to conclude that the sensitivity of H (and therefore

daily ET) to $\Delta(T_0-T_a)$ is dependent not only T_0 but also on the land cover type (and therefore associated roughness parameters), and whether the wet limit has been reached. It can be seen in Figure 4.6 that in two different environments, the sensitivity of SEBS calculated daily ET is dependent on both the land cover and T_0-T_a . For each scenario in Figure 4.6, the wet limit occurs at the apex of the respective curve. Where the wet limit has been reached, the daily ET increases with increasing T_0-T_a ; however, where the wet limit has not been reached, the daily ET decreases with increasing T_0-T_a .

Gibson *et al.* (2011) concluded that SEBS should not be used in mountainous areas or topographically diverse areas as T_0 retrievals are less accurate in this setting and particularly with coarse resolution sensors since the heterogeneity of the T_0 cannot be captured at the appropriate scale. Topographical analysis of potential study areas should be done to minimize the uncertainties that inaccurate T_0 calculations will contribute to the ET results.

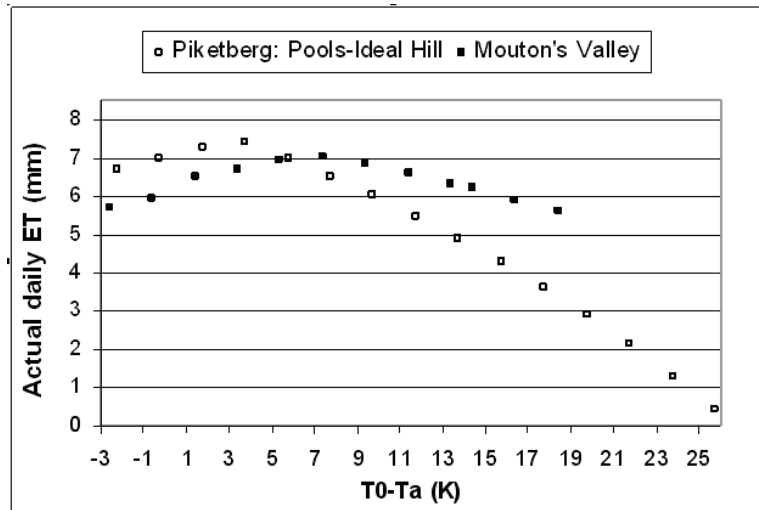


Figure 4.6: The combined effect of T_0-T_a and landcover on daily ET results from Gibson *et al.* (2011). Piketberg: Pools-Ideal Hill is located in a dryland agricultural area and Mouton's Valley is located in a fruit farm in a mountainous area

However, should the uncertainties associated with T_0-T_a be reduced and T_0-T_a is assumed to be correct, H has been shown to be sensitive to fluctuations in this term especially in unstable conditions and in the transition phase where T_0-T_a moves from negative to positive and back again (Su, 2002). According to Su (2002), this sensitivity is suspected to be caused by the current stability correction functions used in SEBS not adequately describing this transition. This was

found to be particularly true in the shrubs and grasslands experiments and more accurate results for agricultural areas were found (Su, 2002). In the similarity theory used in the formulation of the sensible heat flux (Eq 5-7), steady state and horizontally homogeneous conditions are assumed (Gellens-Meulenberghs, 2005) which may not always be good descriptors of natural vegetation and topography in South Africa. It should also be noted that many of the agrometeorological theories and formulae were developed for agricultural crops and not for natural vegetation and perhaps additional parameterization should be considered for those land uses which fall outside of agricultural crops.

Furthermore, since the lag effect of the heating of land differs to the heating of the air and therefore $T_o - T_a$, the time of day of image acquisition may be important and the choice of satellite sensor (such as TERRA which captures images in the morning versus AQUA which captures images in the afternoon) should be considered in this context.

Further considerations are the superior functioning of the AQUA MODIS over the TERRA MODIS sensor. The difference in launch dates allowed for some improvements to be made to the AQUA instrument. Xiong *et al.* (2002) report on the differences between AQUA and TERRA signal-to-noise ratios (SNR) and on-orbit noise equivalent temperature differences. The reported results on both these parameters are that AQUA performs better than TERRA; however, TERRA is performing within the prelaunch standards (with the exception of band 7).

Application to this research:

Since the aim of this research was to minimize uncertainties as far as possible, the selection of homogenous catchments (particularly with respect to topography but also considering landcover) as detailed in Chapter 2, should minimize the uncertainties associated with T_o estimation in the chosen catchments. To minimize the uncertainties for the thermal bands, data from the AQUA sensor was used for the majority of the processing, however, TERRA data was also used for comparative purposes and to indicate the influence of the time of day on ET results due to differing meteorological conditions and differing $T_o - T_a$ due to the differential heating of the land surface and the air.

It has already been stated that $T_o - T_a$ is used in the calculation of the sensible heat flux (H) and it should be noted once again that H is inversely related to ET . As the energy allocated to heating the air increases, so the energy available to evaporate water decreases. This in turn leads to a decrease in evaporative fraction and a decrease in ET .

The effect of using TERRA data versus using AQUA data is illustrated using data from catchment G30G, by way of example. It can be seen that when using TERRA data which is captured in the morning, $T_o - T_a$ is lower than $T_o - T_a$ calculated using AQUA data which is captured in the afternoon. It can also be seen by the negative slope of the TERRA results in Figure 4.7 that the sensible heat flux is always calculated to be at the wet limit when using TERRA data. An indication of the wet limit having been reached is the decrease in sensible heat flux with increase in $T_o - T_a$ whereas the positive slope indicates that the wet limit has not been reached and H is calculated using combination equations (Eqs 5-7). It appears that at TERRA overpass, the transition phase where $T_o - T_a$ moves from negative to positive is not complete, unstable conditions exist and the stability correction functions in SEBS are not suitable. Paradoxically, the fact that the wet limit has been reached does not necessarily mean that the daily estimated ET calculated from using TERRA data will be higher than the AQUA results due to the inverse relationship between H and ET and the fact that AQUA results are generally close to the wet limit and therefore clustered around the wet limit transition.

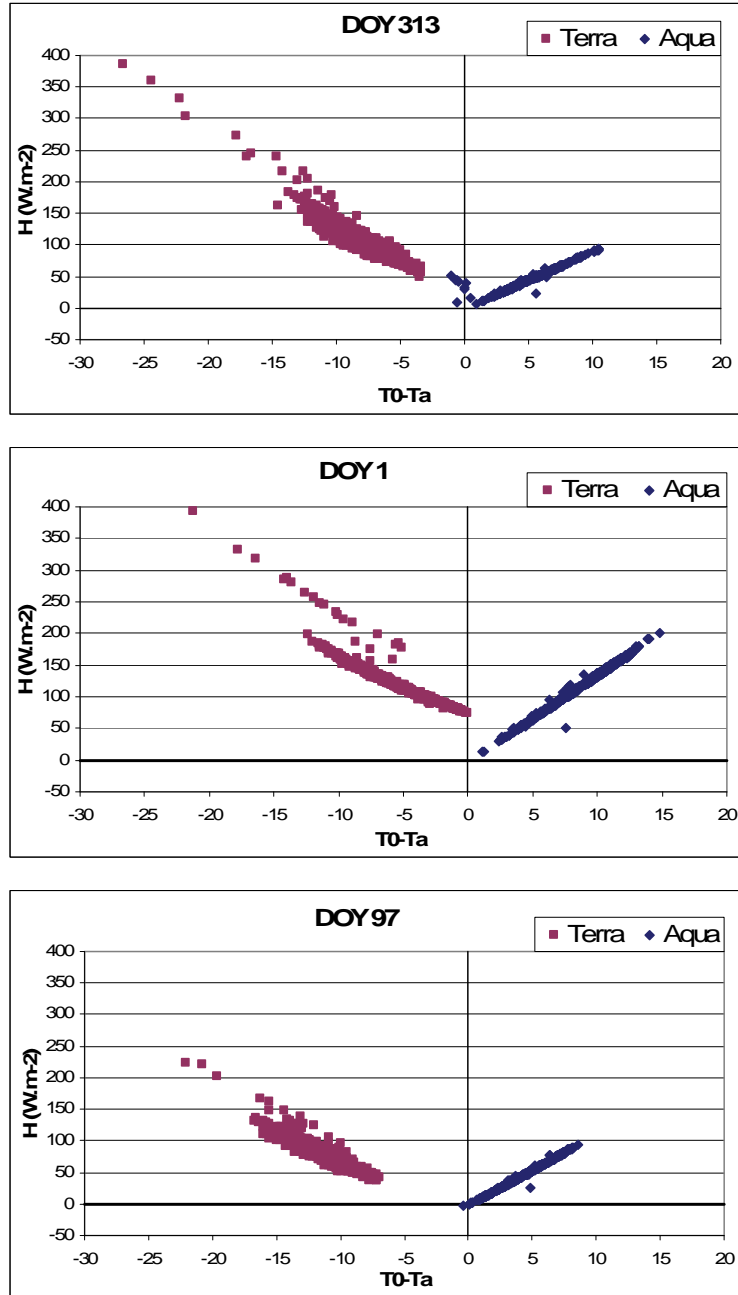


Figure 4.7: Sensible heat flux calculated using TERRA and AQUA data on the same day plotted against $T_0 - T_a$.

These results have very important implications for selecting suitable satellite imagery for a remote sensing energy based ET estimation (particularly with respect to the time of day of image capture) and further research is required on this topic.

4: Roughness length and displacement heights

Roughness length (z_0) is a measure of the aerodynamic roughness of a surface and is related to but not equal to the height of the roughness elements. It is also a function of the shape and density distribution of the roughness elements. For example, a grassy plain has a lower roughness than an area with many trees and buildings (Kipp & Zonen, 2005). Zero plane displacement height is defined as the height above the ground at which zero wind speed is achieved due to friction caused by roughness elements.

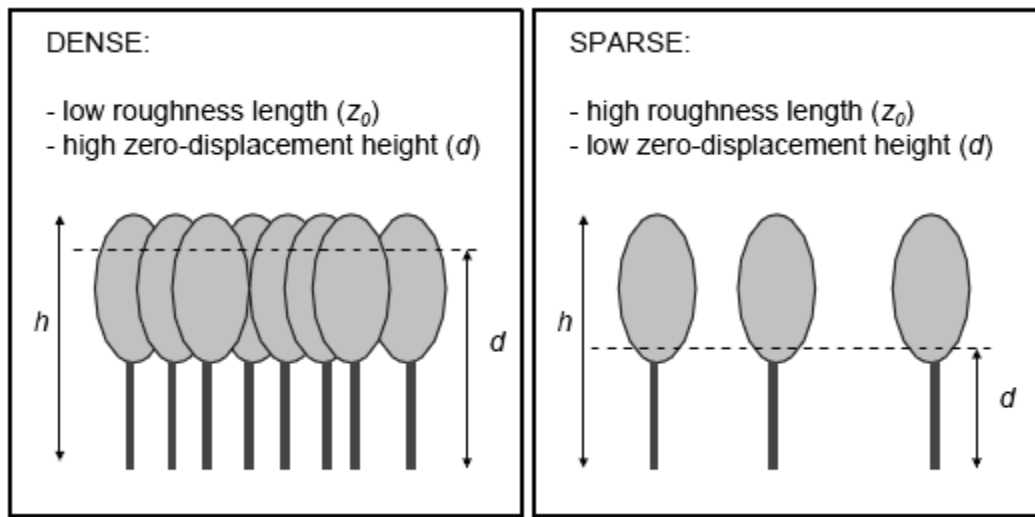


Figure 4.8: Dependence of roughness length and displacement height on height and density of roughness elements (e.g. trees) (Kipp & Zonen, 2005)

Within SEBS, it can be seen in Eqs 5 & 6 that roughness lengths for momentum and heat transfer and displacement height are used to derive the sensible heat flux. z_{0m} can be obtained from the literature or can be empirically derived from the remote sensing vegetation inputs. If z_{0m} and d_0 are derived from remote sensing vegetation inputs (the approach used by Gibson *et al.* (2009)), firstly the roughness length for momentum transfer is estimated using the method by Su & Jacobs (2001) in Hailegiorgis (2006):

$$z_{0m} = 0.005 + 0.5 \left(\frac{NDVI}{NDVI_{max}} \right)^{2.5} \quad (12)$$

Next the vegetation height (h) is calculated from the roughness height for momentum transfer followed by the zero plane displacement height using the method of Brutsaert (1982):

$$h = \frac{z_{0m}}{0.136} \quad (13)$$

$$d_0 = \frac{2}{3}h \quad (14)$$

It is apparent that if Eqs 12-14 are used to calculate z_{0m} and d_0 , then areas which have a low NDVI will be assigned a low roughness length, a low canopy height and a low displacement height. Although this assumption may generally hold true in certain irrigated agricultural regions, it does not allow for the case of semi-arid environments where shrubs and fynbos type vegetation have a low NDVI during the hot dry summer but the canopy height does not follow a seasonal curve in the way that NDVI does. In this scenario, the roughness length, canopy height and displacement height are independent of NDVI and should not vary throughout the year with NDVI. Therefore, although it may be acceptable to use Eqs 12-14 in certain environments within the South African context, they should not be used for natural vegetation or dryland agriculture. In these environments, literature values should be used. It is particularly important to note that the roughness length is used together with T_0 (reportedly the parameter to which SEBS is most sensitive) in the calculation of H . The combined effect of uncertainties in T_0 , together with inaccuracies in z_{0m} leads to greater inaccuracies in the calculation of H and therefore ET .

Furthermore, the type of weather station and the reference height at which wind speed is measured is critical to the correct implementation of the SEBS model particularly in tall canopies. In South Africa, the installation of automatic agrometeorological weather stations complies with standards set by the World Meteorological Organisation except in the height measurement of wind speed and direction. South African agrometeorological standards state that wind speed and wind direction are measured at 2 m above the surface (ARC-ISCW, 2010) in contrast to the South African Weather Service (SAWS) which measures wind speed and direction at 10 m above the surface. A problem arises when using data from agrometeorological

weather stations in canopies of 3 m or higher (where $d_0 > 2$), as is the case with orchards in the study area. To derive the sensible heat flux the calculation of $z - d_0$ is required in Eqs 5 & 6, where z is the reference height at which wind speed is measured (2 m, in the case of an agrometeorological weather station). When measuring wind speed at 2 m, and solving for H using Eqs 5-7, a situation arises where $z < d_0$, and the \ln of a negative number needs to be solved. Additionally, the SEBS model was shown by Gibson *et al.* (2011) to exhibit high sensitivity to d_0 as $z-d_0$ approaches zero. In an area where field crops with a low canopy height predominate, the use of an agrometeorological weather station is appropriate. However, where tree crops and natural vegetation with a canopy height exceeding 2.7 m are found, weather stations which measure wind speed at 10 m (such as SAWS weather stations) are appropriate.

Application to this research:

Reference heights: In the G30G catchment where low fynbos dominates and tall vegetation is rare, the ARC-ISCW weather station Sandberg which measures wind speed at 2 m above the surface could be used in the SEBS model. In the P10A catchment, the presence of thicket and taller vegetation meant that the 2 m reference height from ARC-ISCW weather stations was not suitable. For this reason the SAWS weather station at Grahamstown airfield which measures wind speed at 10 m above the surface was selected and meteorological data was obtained from SAWS for input into the SEBS model. However, since the SAWS weather station does not measure radiation, the ARC-ISCW weather station at Rockhurst located outside the catchment was used for radiation inputs.

During the course of a field visit to the P10A catchment, (Appendix I) it became apparent that using the NDVI to estimate vegetation height and therefore roughness parameters was not a suitable method so the allocation of roughness lengths based on landcover approach was followed. The National Land Cover 2000 map (Van den Berg *et al.*, 2008) was used as a basis and using high resolution SPOT imagery, the NLC 2000 map was modified by visual interpretation to delineate landcovers on the basis of roughness characteristics. The footprint of the MODIS pixel was then overlain on the landcover map and landcover covering the largest area within each MODIS pixel was assigned to each MODIS pixel. Roughness lengths and displacement heights were assigned to each new landcover using literature values for similar

landcovers. This process can be seen in Figure 4.9. It can be seen that this process is highly subjective and there are some flaws in selecting a roughness parameter for a pixel purely based on the majority landcover within the pixel, nevertheless in the absence of a better methodology suitable at MODIS pixel resolution, this may be the best approach.

The importance of using a correct z_0 is shown in Figures 4.10-4.12 where three z_0 values are assigned and the SEBS model is run for each of these z_0 values keeping all other input parameters unchanged. Three different dates are selected to show the sensitivities at high T_0-T_a , T_0-T_a close to zero and negative T_0-T_a . It can be seen in Figure 4.10 that the sensible heat flux is most sensitive to high z_0 values at high T_0-T_a values. As z_0 and T_0-T_a decrease, so too does the sensitivity of H to these values. In Figures 4.11 & 4.12 where the wet limit begins to be reached, the slope changes and the sensitivity to T_0-T_a and z_0 is less predictable. This is due to the fact that at the wet limit T_0-T_a and z_0 are not used as direct inputs into the calculation of the sensible heat flux since Eq 3 is used for this calculation. It can therefore be said that at low T_0-T_a , the importance of a correct z_0 is less critical than at a high T_0-T_a where the accuracy of z_0 is very important particularly in area with high roughness lengths, generally corresponding to taller vegetation.

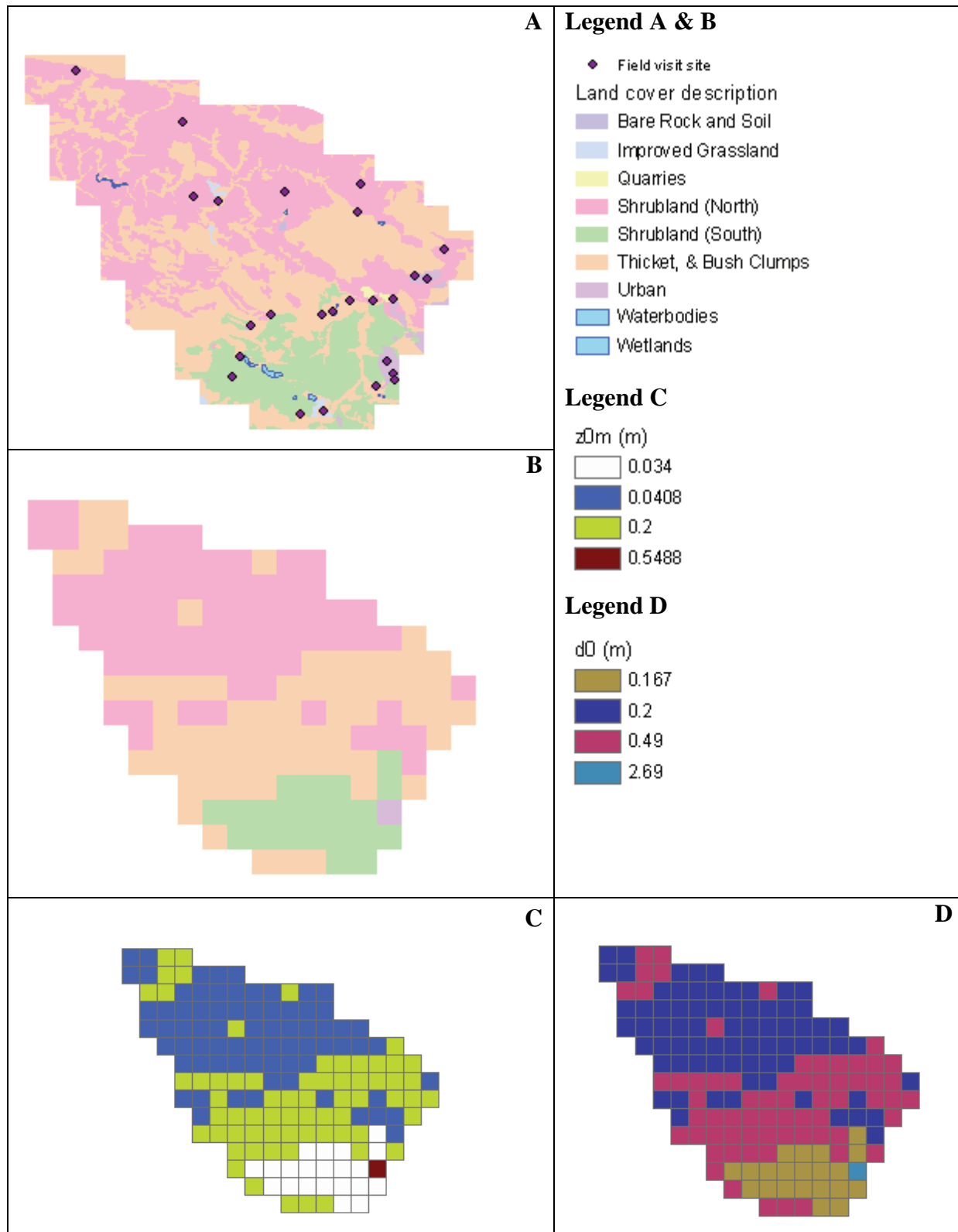


Figure 4.9: The process of allocating z_0 and d_0 values in the P10A catchment. A. Modified landcover map, B. Landcover by MODIS pixel, C. Allocated roughness lengths and D. Displacement heights

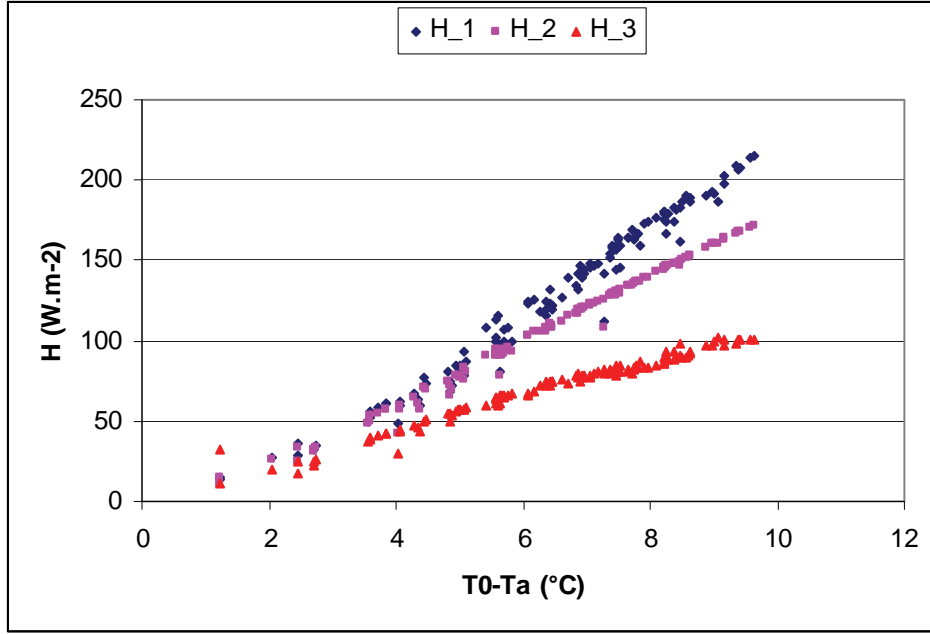


Figure 4.10: Summer scene, P10A, DOY 017: Sensitivity of sensible heat flux to z_{0m} and $T_0 - T_a$. H_1 : z_{0m} is set to 1m; H_2 , z_{0m} is set to 0.5m; and H_3 , z_{0m} is set to 0.1m. It can be seen that sensitivity of H to z_{0m} increases with increasing $T_0 - T_a$

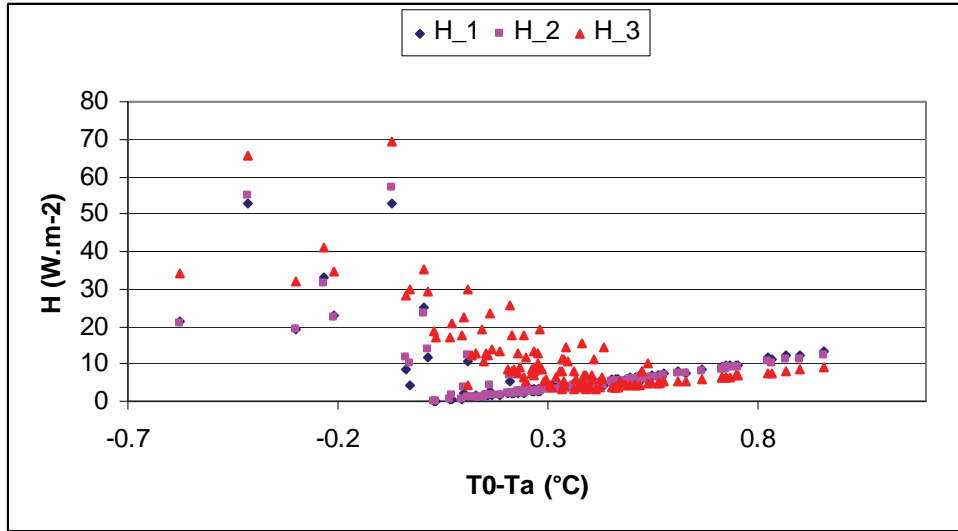


Figure 4.11: Winter scene, P10A, DOY 217: Sensitivity of sensible heat flux to z_{0m} and $T_0 - T_a$. H_1 : z_{0m} is set to 1m; H_2 , z_{0m} is set to 0.5m; and H_3 , z_{0m} is set to 0.1m. It can be seen that sensitivity of H to z_{0m} is non linear around $T_0 - T_a = 0$

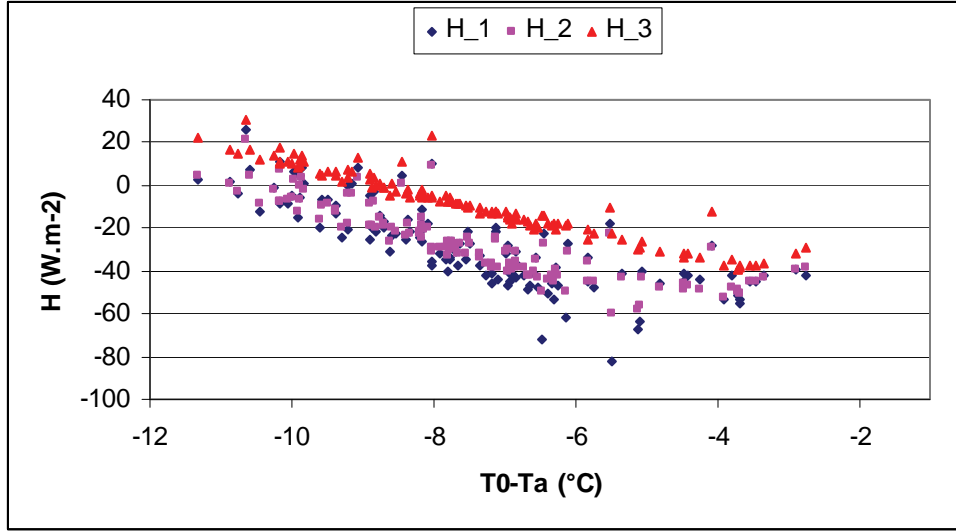


Figure 4.12: Winter scene, P10A, DOY 185: Sensitivity of sensible heat flux to z_{0m} and T_0-T_a . H_1 : z_{0m} is set to 1m; H_2 , z_{0m} is set to 0.5m; and H_3 , z_{0m} is set to 0.1m. It can be seen that the slope is negative in this instance indicating that the wet limit has been reached at low T_0-T_a

Results

The research was an iterative process as the importance of addressing some of the items above was only discovered through selecting images, running the model, analyzing the results and then adapting the methodology and input data. Due to the iterative nature and the volume of data involved, it is very difficult (and not particularly helpful) to present the results of all iterations but rather to present results after all the adaptations to input data, image selection, etc. had been made as discussed.

The catchment average daily ET results from the SEBS model are shown in Figures 4.13 & 4.14 plotted against reference ET for G30G and P10A respectively. It can be seen that the SEBS model results in ET which is consistently at, or higher than, than reference ET_0 . This is true for both the AQUA and TERRA. Despite all the modifications to reduce uncertainties, as with the results of Gibson *et al.* (2009), the SEBS model appears to overestimate catchment ET .

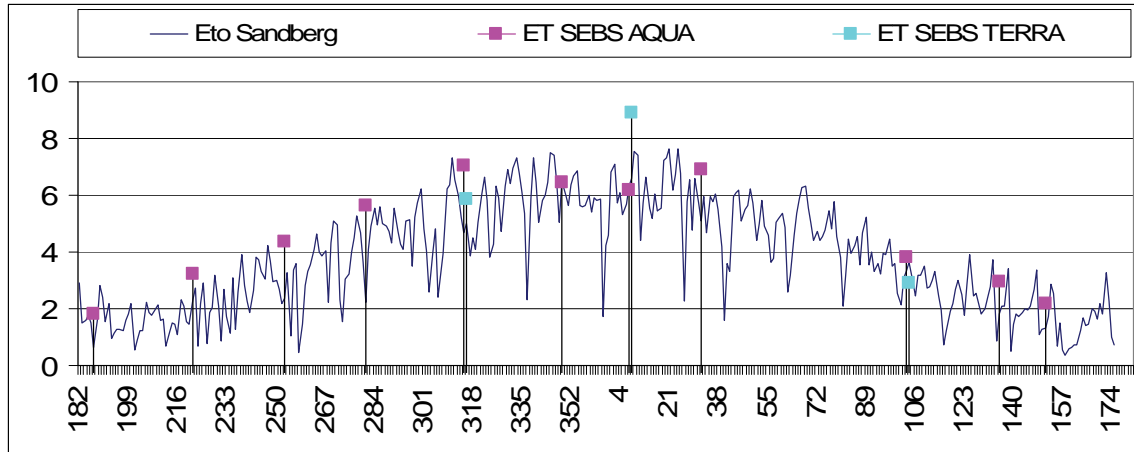


Figure 4.13: Catchment average ET calculated for G30G using the SEBS model with AQUA and TERRA data and plotted against ET_0 calculated from the Sandberg weather station for the study period (July 2006-June 2007)

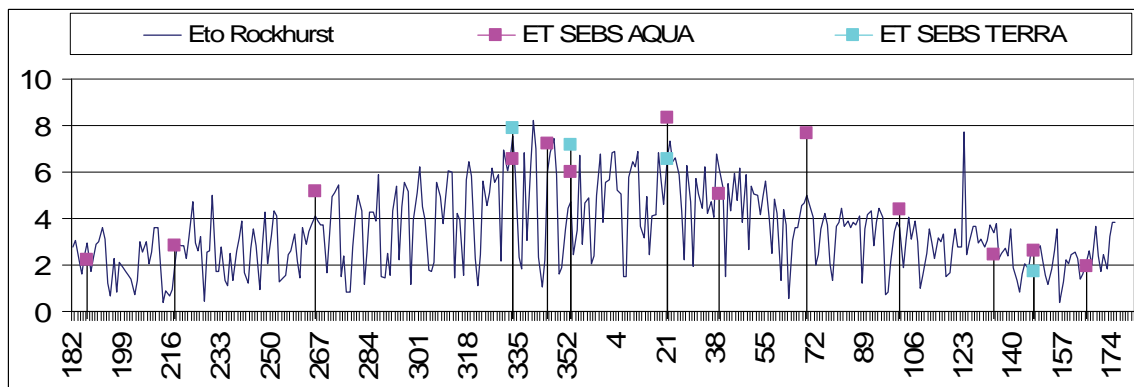


Figure 4.14: Catchment average ET calculated for P10A using the SEBS model with AQUA and TERRA data and plotted against ET_0 calculated from the Rockhurst weather station for the study period (July 2006-June 2007)

It can be seen in Figure 4.13 that in G30G in hot dry summer months the results do not appear to reflect the limit in water availability which is known to occur in that region (GEOSS, 2006). The SEBS calculated ET is simply highest when the energy or atmospheric demand is the highest and lowest where the energy or atmospheric demand is the lowest. This dependence on energy or atmospheric demand can be seen to a lesser extent in P10A (Figure 4.14).

In Figures 4.15 & 4.16, the SEBS ET AQUA results are plotted against $T_0 - T_a$ for individual pixels for G30G and P10A respectively. The range in estimated ET in the catchment for each selected day throughout the study period can be seen and the high ET in G30G in the summer months is once again noted for all pixels in the catchment despite water availability limitations.

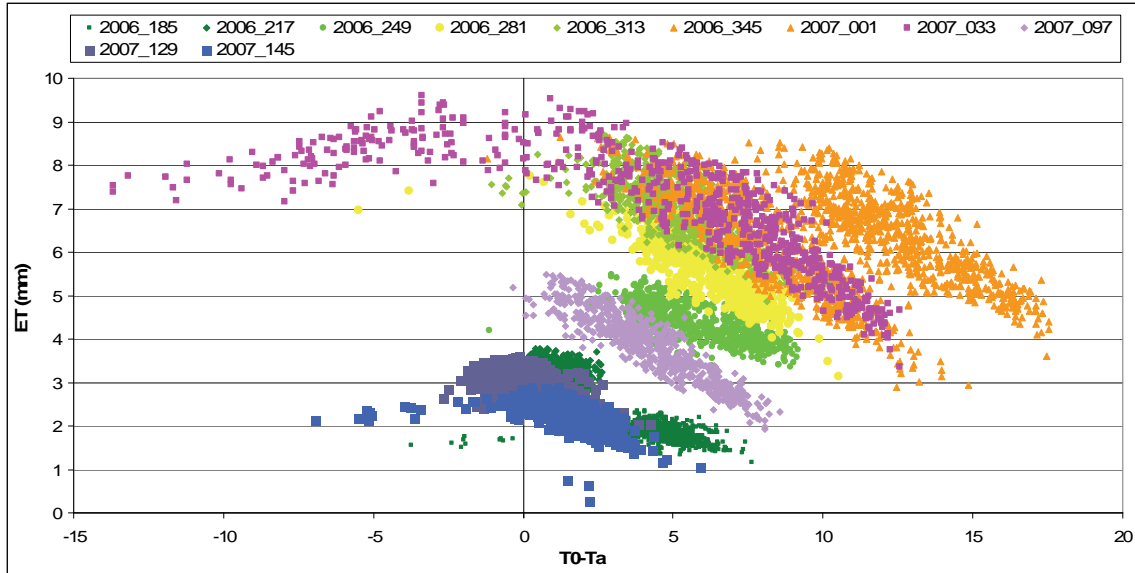


Figure 4.15: AQUA SEBS ET results for each date processed for the G30G catchment plotted against $T_0 - T_a$

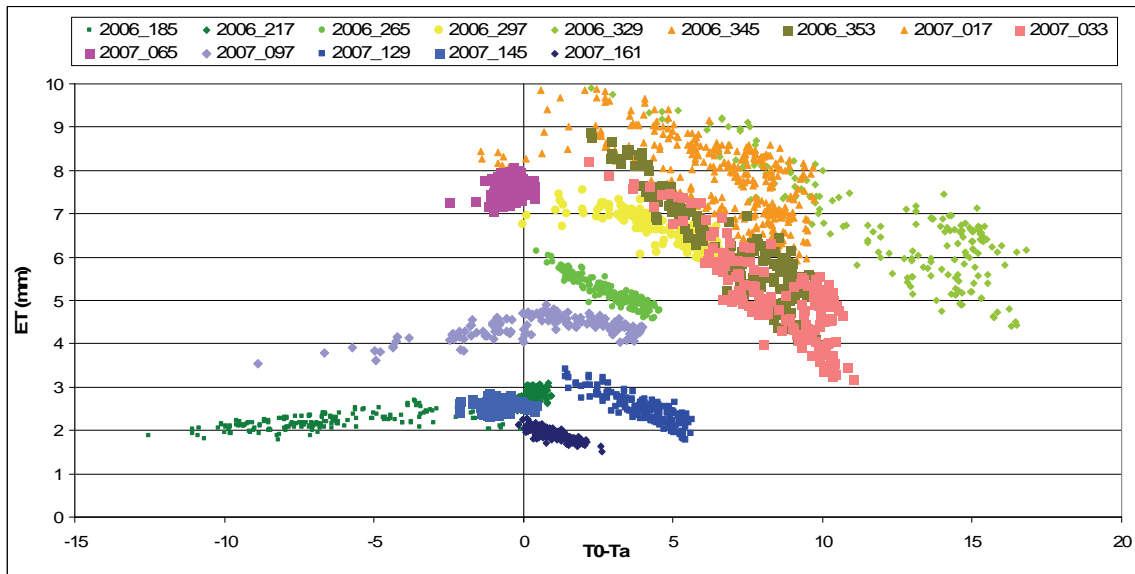


Figure 4.16: AQUA SEBS ET results for each date processed for the P10A catchment plotted against $T_0 - T_a$

Despite the best efforts to address the uncertainties and limitations highlighted by Gibson *et al.* (2009) and Gibson *et al.* (2011) in the research methodology, the *ET* still appears to be overestimated in both the G30G and P10A catchments. Briefly unpacking a high *ET* result in SEBS, it can be seen that:

1. A high ET is caused by a high evaporative fraction.
2. A high evaporative fraction is caused by energy being partitioned to the latent heat flux rather than the sensible heat flux.
3. Since the SEBS model solves the latent heat flux as the residual of the energy balance, the calculation of a sensible heat flux which is too low is the most contributing factor to high ET in SEBS.

The sensitivity of H to $T_0 - T_a$ and z_0 has already been discussed. Figures 4.17 & 4.18 show the evaporative fraction results for each AQUA scene plotted against $T_0 - T_a$. It can be seen that in the case of $T_0 - T_a$ greater than zero, as $T_0 - T_a$ increases, the evaporative fraction decreases. This is in line with the sensitivity of H to $T_0 - T_a$ as illustrated earlier in the text and this sensitivity may be exacerbated by incorrect roughness lengths. What is also apparent from Figures 4.17 & 4.18 is that on no occasion does the evaporative fraction fall below 0.3 and the majority of the pixels fall above 0.7 for both the G30G and P10A catchments regardless of the different hydrological regimes (median 0.834 for G30G and 0.876 for P10A respectively). This leads to the conclusion that regardless of the accuracy of the input data (excluding image resolution) or the environment, these results indicate that the SEBS model remains unable to allocate enough energy to the sensible heat flux. This confirms the results of Gibson *et al.* (2009) that SEBS is overestimating ET , particularly in natural landscapes.

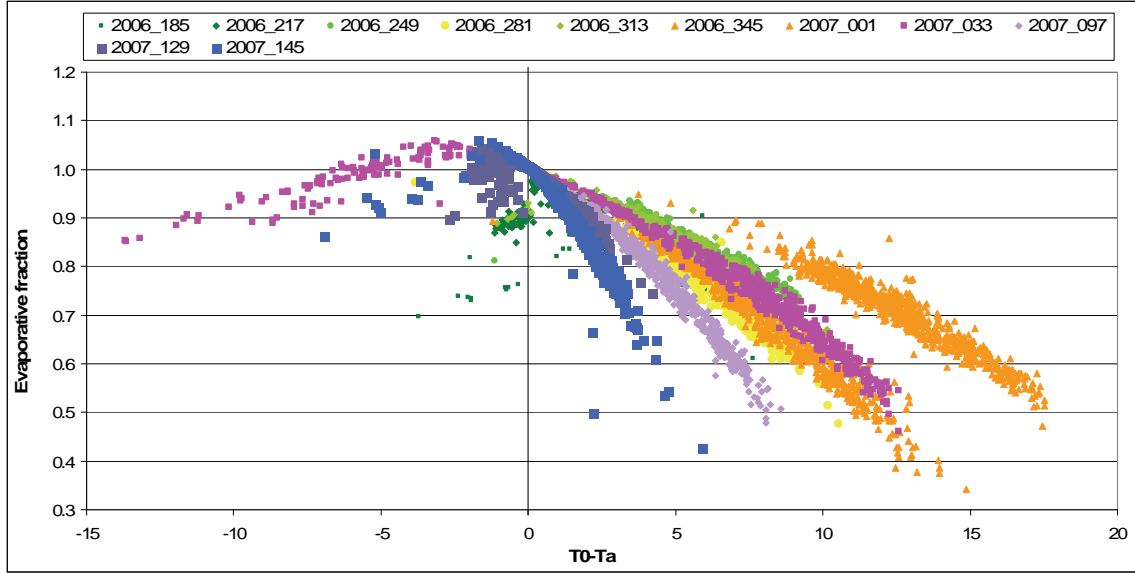


Figure 4.17: AQUA SEBS evaporative fraction results for each date processed for the G30G catchment plotted against $T_0 - T_a$

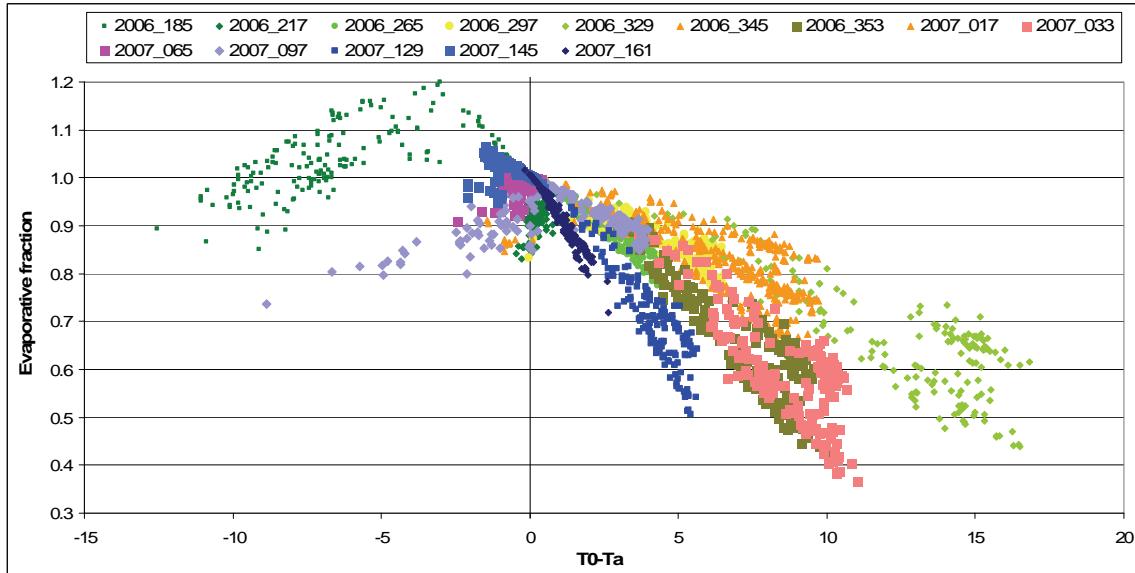


Figure 4.18: AQUA SEBS evaporative fraction results for each date processed for the P10A catchment plotted against $T_0 - T_a$

In a recent paper by Timmermans *et al.* (2011), of which the developer of SEBS is one of the co-authors, it is stated that “the uncertainties in the sensible heat flux arise due to a misparameterization of the roughness height for heat. In the original SEBS formulation the roughness height for heat is only valid for short vegetation.” The calculation of the roughness height for heat transfer (z_{0h}) is based on z_{0m} and the original formulation is given in Su (2002).

Timmermans *et al.* (2011) have added an additional parameterization for tall vegetation to the SEBS algorithm to account for the misparameterization in the original formulation. This paper appeared online on 16 March 2011 and is still undergoing the peer review process and time did thus not allow for any changes to be incorporated in this research.

Field validation was not possible in this research project due to budgetary constraints but the results of the SEBS model are compared to the results of other remote sensing *ET* models in the same catchments. Unfortunately the results of the Sandveld SEBAL project were not available at the time of writing, so the ET-API method was used in both G30G and P10A.

Daily catchment average *ET* using the ET-API method for G30G and P10A are shown in Figures 4.19 & 4.20 plotted against ET_0 . It can be seen that *ET* is consistently below the ET_0 and in G30G the summer peak in *ET* as estimated by SEBS is not seen. This is in line with expectations since at that time in the study period there was no rainfall and the stress on groundwater in the area is well documented (GEOSS, 2006). Also apparent is that the highest daily *ET* in G30G does not exceed 2 mm/day in stark contrast to the SEBS results which were rarely below 2 mm/day (Figure 4.19). In P10A (Figure 4.20), *ET* follows ET_0 more closely and higher daily *ET* is seen in the summer months due to the availability of both energy and water. Since the results of the ET-API method appear to show realistic catchment *ET* results, these will be used in the catchment water balance results.

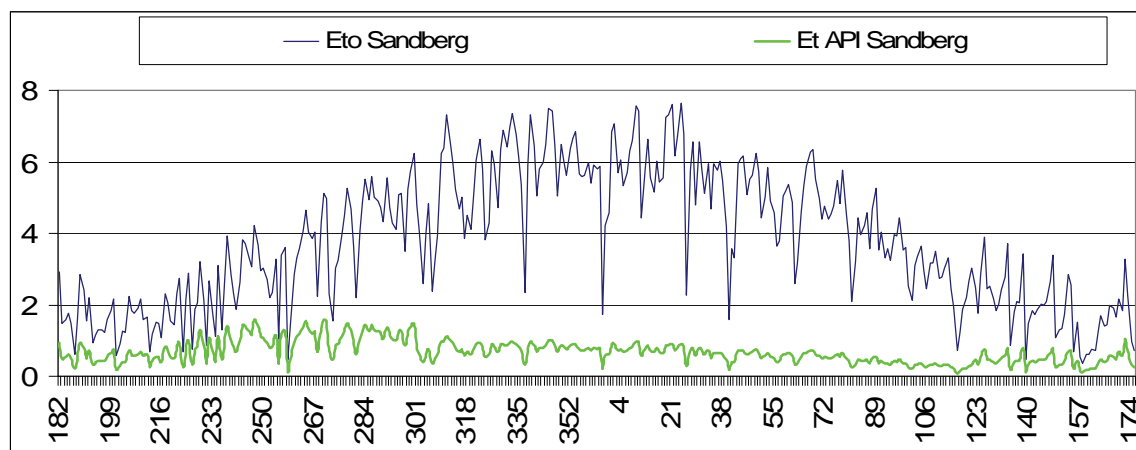


Figure 4.19: Catchment average daily *ET* for G30G from the ET-API method compared with ET_0 from the Sandberg weather station for the study period (July 2006-June 2007)

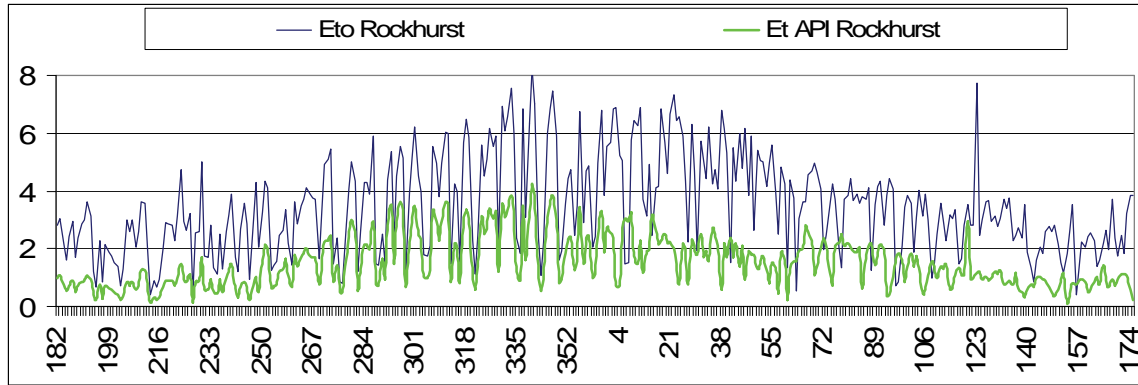


Figure 4.20: Catchment average daily ET for P10A from the ET-API method compared with ET_0 from the Rockhurst weather station for the study period (July 2006-June 2007)

Chapter 5 – Precipitation

The ARC-ISCW creates rainfall grids using a combination of automatic weather station rainfall data and downloaded satellite rainfall data. Each grid can be used for the identification of the actual decadal rainfall total in mm across South Africa and can be summed to obtain the total rainfall over specified time periods (ARC-ISCW, 2005). The methodology for plateau and coastal regions given in the grids' metadata is as follows:

Rainfall data from about 550 automatic stations is extracted.

Satellite rainfall estimates are downloaded from African Data Dissemination Service.

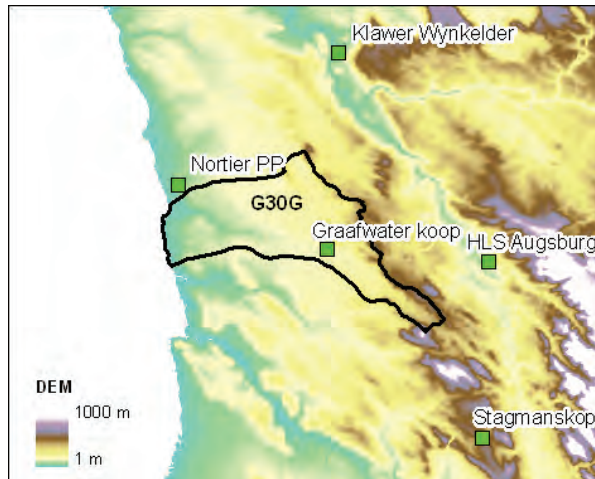
The interpolation method assigns a rainfall value to a specific point based on the measured rainfall at the five closest rainfall stations and the satellite rainfall estimate.

Rainfall data from stations are combined with the satellite rainfall estimate data for 11 500 points spread evenly over South Africa.

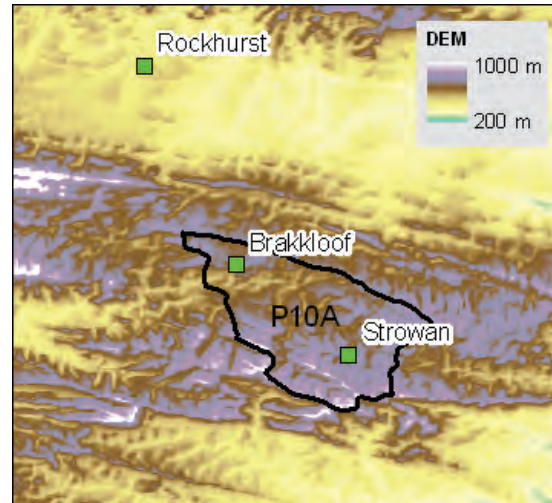
New combined estimate values are interpolated through the IDW method (ARC-ISCW, 2005).

There is, however, a resolution limitation pertaining to the use of this dataset. The resolution of the rainfall grids is 1 km and the resolution of the original satellite rainfall estimate is 8 km. In addition, weather stations are irregularly spaced over South Africa which should allow for regional modelling rather than analyzing data at a microclimate scale (ARC-ISCW, 2005).

Any rainfall measurements collected (via manual weather stations, SAWS or private weather stations) which have not already been included in the ARC-ISCW rainfall interpolation grid will be used to validate the ARC-ISCW dataset. In Figure 5.1 the manual and private weather stations selected for validating the ARC-ISCW rainfall grid are shown. In G30G, only ARC-ISCW manual weather stations were used and all fell outside the G30G catchment. In P10A, two private manual rain gauges were found within the P10A catchment and the ARC-ISCW automatic weather station at Rockhurst which was not used in the making of the grid were used to validate the results.



A: G30G



B: P10A

Figure 5.1: Rain gauges used to validate ARC-ISCW grid results for G30G (A) and P10A (B)

The summed ARC-ISCW grids are validated by extracting the pixel values on which the stations being used to validate the result are located. These values are plotted against recorded total study period and monthly rainfall values at each of the validating stations in Figures 5.2 & 5.3 for G30G and P10A respectively. Likewise, Tables 5.1 & 5.2 show the total study period and monthly r^2 values for each of the validating stations in G30G and P10A respectively.

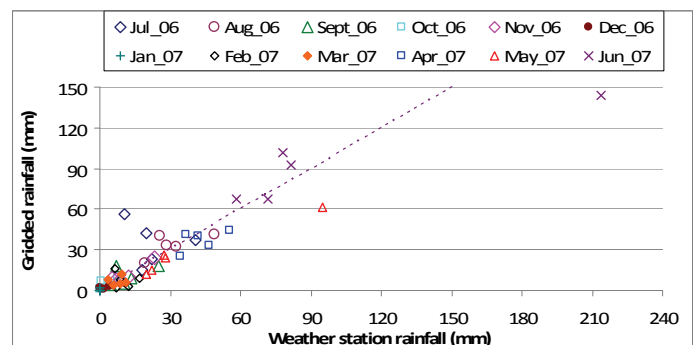
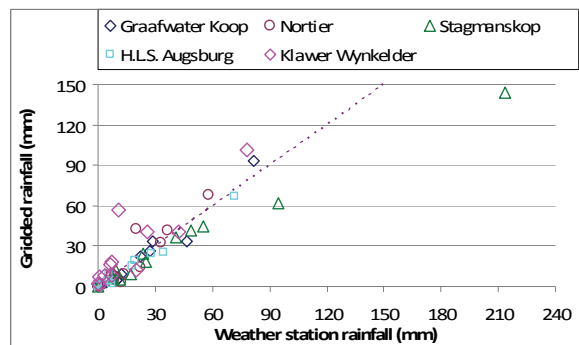


Figure 5.2: ARC-ISCW grid values against rainfall measured at the validating stations in G30G for study period totals (on the left) and monthly values (on the right)

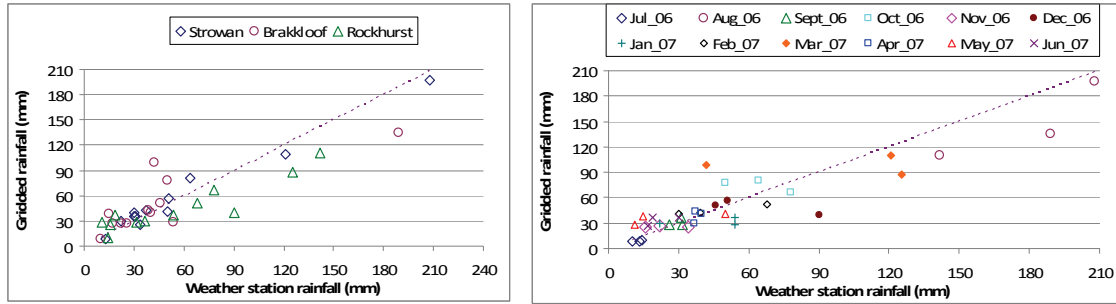


Figure 5.3: ARC-ISCW grid values against rainfall measured at the validating stations in P10A for study period totals (on the left) and monthly values (on the right)

Table 5.1: r^2 values showing goodness of fit between weather station data and ARC-ISCW grid results at station level (above) as well as per month (below) for G30G

Weather station	R^2
Graafwater Koop	0.956
Nortier	0.869
Stagmanskop	0.987
H.L.S. Augsburg	0.978
Klawer Wynkelder	0.782

Month	R^2	Month	R^2	Month	R^2
Jul_06	0.040	Nov_06	0.908	Mar_07	0.014
Aug_06	0.482	Dec_06	0.805	Apr_07	0.312
Sept_06	0.267	Jan_07	0.000	May_07	0.958
Oct_06	0.425	Feb_07	0.010	Jun_07	0.847

Table 5.2: r^2 values showing goodness of fit between weather station data and ARC-ISCW grid results at station level (above) as well as per month (below) for P10A

Weather station	R^2
Strowan	0.973
Brakkloof	0.677
Rockhurst	0.841

Month	R^2	Month	R^2	Month	R^2
Jul_06	0.700	Nov_06	0.001	Mar_07	0.005
Aug_06	0.783	Dec_06	0.843	Apr_07	0.161
Sept_06	0.189	Jan_07	0.150	May_07	0.529
Oct_06	0.588	Feb_07	0.999	Jun_07	0.304

It can be seen in Figures 5.2 & 5.3 that there is a good correspondence between the ARC-ISCW grid and the validation stations for both G30G and P10A. More in-depth examination of the

results in Tables 5.1 & 5.2 shows that in G30G, the weather station which best correlates with the ARC-ISCW grid is Stagmanskop and the weakest correlation is found at Klawer Wynkelder. In P10A, the weather station which best correlates to the ARC-ISCW grid is Strowan and the weakest correlation is at Brakkloof. It can be seen in both G30G and P10A that the best correlations occurred in the months with the highest rainfall. The ARC-ISCW grid appears to predict catchment rainfall with a high degree of accuracy; however, the limited availability of validation results is noted.

Chapter 6 – Groundwater

G30G

The geological setting of quaternary catchment G30G is shown in Figure 6.1. The ‘bedrock’ of quaternary catchment G30G comprises the lowest (oldest) formation of the Table Mountain Group, namely the Piekenierskloof Formation (C1Q1R). It consists of quartzitic sandstone and conglomerate. The most recent description of Sandveld geology has been documented by the Council for Geoscience (de Beer, 2003).

Within the Table Mountain Group the Piekenierskloof Formation in places is an excellent aquifer due to the fracturing and its great thickness. The groundwater quality with the Piekenierskloof Formation is also very good with a low TDS content.

Whilst the Graafwater Formation is considered a poor aquifer (even an aquitard in places), the arenaceous: argillaceous ratio does vary throughout the formation. However, borehole yields are typically low and the water quality is poor.

The Peninsula Formation is an extremely important hydrogeological unit and has proven to be an excellent aquifer in places. Its competent character and gritty, pebbly sandstones give it a favourable permeability and transmissivity. The water quality from the Peninsula Formation is typically very good with a low TDS. However, the pH is low and is considered quite an “aggressive” water which benefits from lime stabilization prior to use.

The sandy Cenozoic cover is agriculturally the most intensively exploited succession in the Sandveld. Its high porosity and high horizontal permeability result in high borehole yields within these primary aquifer deposits. Interestingly, the vertical recharge reduces to almost zero in the western portion of the study area, yet the primary aquifer is very high yielding in this area. This is attributable to the high groundwater flows within the fractured bedrock that result in recharge occurring from beneath the sands in an upward direction. The highest borehole yields occur where the primary aquifer is drilled into, above these structurally favourable features that

occur in the bedrock. In general terms the water quality deteriorates from the mountainous recharge areas in the east of the study area towards the low lying, low recharge coastal region.

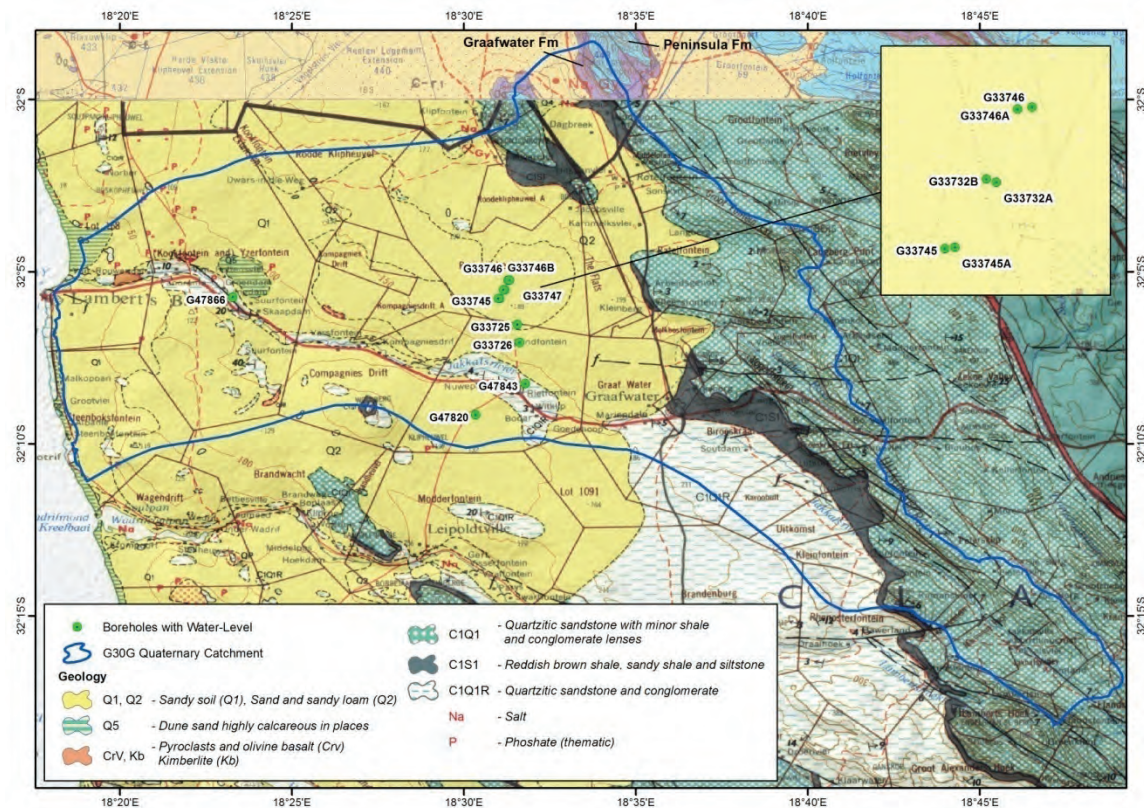


Figure 6.1: Geology of G30G catchment and surrounds

The Sandveld is a low rainfall area where significant groundwater abstraction occurs for agricultural purposes and the town of Graafwater is entirely dependent on groundwater for domestic and industrial supply. Sensitive and important ecosystems in the area are showing varying degrees of impact (GEOSS, 2006). Figure 6.2 shows the groundwater levels in selected boreholes in G30G for the study period (locations shown in Figure 6.1). These are monitoring boreholes thus abstraction from nearby boreholes may contribute to water-level fluctuations. Borehole G47843 shows a 4 m drop in water level in response to the dry summer conditions but recovery associated with rainfall is rapid. This borehole is located in the Piekenierskloof Formation (C1Q1R) and as an unconfined aquifer is subject to direct recharge from rainfall. It can be seen that the groundwater levels in the Graafwater wellfield (boreholes labelled G33*), all found in sandy soil (Graafwater Primary Aquifer, Q1 & Q2). Water levels remain constant throughout the study period, fluctuating by less than 0.2 m even during the dry summer months.

Recovery of water level after the rainfall event in November 2006 can be seen in the December 2006 water levels for these boreholes. From drilling in the area, it has been noted that a clay layer is often found beneath the sand acting as a confining layer. Recharge of a confined aquifer is often indirect from beneath or lateral which may explain the low range of variation for many of the boreholes, and a delayed response of recharge from rainfall.

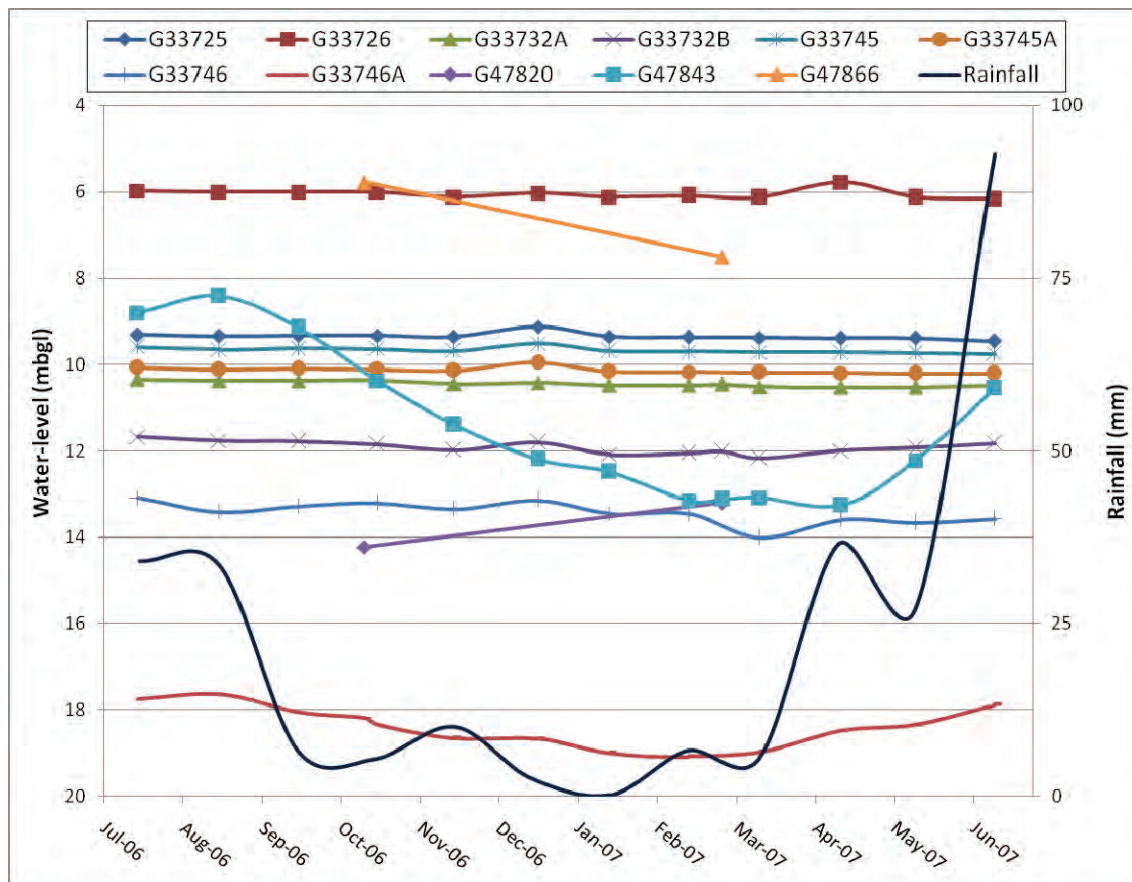


Figure 6.2: Groundwater levels in G30G versus ARC-ISCW catchment average rainfall

P10A

The geology of quaternary catchment P10A is in shown in Figure 6.3 and summarized in Table 6.1.

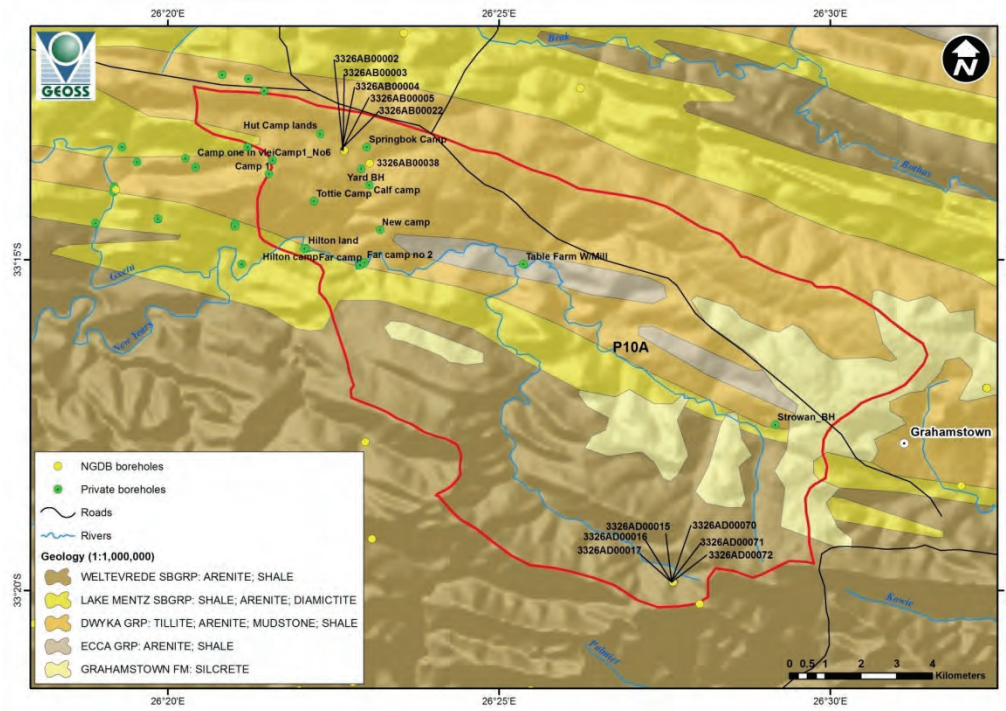


Figure 6.3: Geological map of P10A and surrounds also showing borehole locations

Table 6.1: Lithostratigraphy of catchment P10A

Super-Group	Group	Sub-Group	Formation	Symbol
Tertiary			Grahamstown	Tg
Karoo	Ecca			Pr
	Dwyka			C-Pd
Cape	Witteberg	Lake Mentz		Dℓ
		Weltevrede		Dw

The oldest rock types within quaternary catchment P10A belong to the Weltevrede Sub-group (DW) of the Witteberg group of the Cape Super-group. The Weltevrede Sub-group comprises quartzite, sandstone, siltstone and shale. Overlying the Weltevrede Sub-group is the Lake Mentz Sub-group (Dℓ) (also of the Witteberg Group). The Lake Mentz Sub-group comprises shale, sandstone and diamictite (a poorly or non-sorted conglomerate with a wide range of clust sizes). Overlying the Lake Mentz Sub-group are the rocks of the Dwyka Group (Karoo Super-group). The Dwyka Group (C-Pd) comprises tillite, sandstone, mudstone and shale. Overlying the Dwyka Group is the Eccca Group (Pr) which is also part of the Karoo Super-group.

The Ecca Group consists mainly of sandstone and shale. The youngest rock type in the area is the Tertiary age silcretes of the Grahamstown Formation. Silcrete is a hard and resistant material; it appears similar to quartzite and is formed by silica dissolving and re-solidifying, almost as 'cement'. The lithologies extend in a north-easterly/south-westerly direction with a clear synclinal trough, with the same trend.

Hydrogeologically the Weltevrede Sub-group (Dw) is a poor aquifer due to the presence of siltstone and shale. However the arenaceous: argillaceous ratio can vary throughout the Sub-group and it may be feasible to drill low yielding boreholes in the more arenaceous regions, although water quality is likely to be poor. The Lake Mentz Sub-group (Dl) is a non-aquifer due to the extensive presence of clay. The Dwyka Group (C-Pd) is also a non-aquifer in this study area. The wide range in clust sizes renders an extremely low transmissivity. The overlying Ecca Group (Pr) comprises a high portion of shale and is generally known as a non-aquifer. The silcrete capping (Tg) of the Grahamstown Formation, due to its limited thickness, is also considered a non-aquifer.

In summary the geological setting does not favour high groundwater potential and the groundwater that does occur is probably of poor quality, even though the rainfall is relatively high in the south-eastern corner of the study area. The Weltevrede Sub-group of the Witteberg Group probably has the best groundwater potential of all the lithologies. The Department of Water Affairs hydrogeological map indicates a water quality (electrical conductivity) of 70-300 mS/m for the Witteberg Group and 300-1000 mS/m for the other lithologies in the north-eastern portion of the study area.

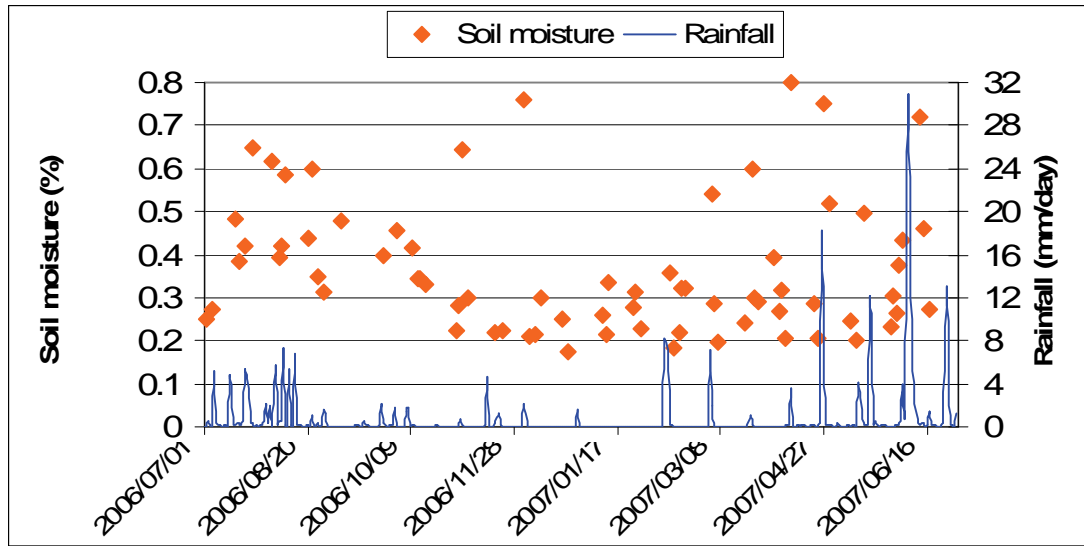
Based on a hydrocensus of the study area the poor groundwater potential of the area is confirmed. Very little use is made of groundwater within the study area. Appendix II presents the results of the hydrocensus. The National Groundwater Archive (NGA) boreholes obtained within quaternary catchment P10A as shown in Figure 6.3 could not be located in the field.

Chapter 7 – Soil moisture

The Technical University of Vienna has aimed to address the needs of the hydrological community by producing a medium resolution soil moisture dataset using Synthetic Aperture Radar (SAR) data. The operational soil moisture product is now available for the Southern African Development Community (SADC) region and for Australia. The dataset at 1 km resolution is produced from twice weekly measurements to capture the variability in soil moisture patterns. The 1 km soil moisture dataset has been provided as part of the SHARE European Space Agency DUE TIGER innovator project and aims to provide operational free of charge soil moisture monitoring service for the SADC region. Data is available at <http://www.ipf.tuwien.ac.at/radar/share/> (Doubkova *et al.*, 2009).

A data request was sent to the SHARE team and data was made available for download via a ftp site. The first step was to only select those datasets which covered the entire catchment and datasets which only partially covered the catchment were excluded from analysis. In addition, those datasets containing many no data values were excluded from analysis. The data was then compiled per month with the dates of each image capture retained for each individual dataset. Records which contained no data values were excluded from the analysis for each dataset in that particular month. The average catchment value for soil moisture was calculated for each dataset in a particular month meaning that for each month there could be 1-5 catchment average soil moisture values for a month dependent on the number of datasets that were retained through the above process. The average soil moisture results for G30G and P10A are plotted against rainfall and ET_0 in Figures 7.1 & 7.2 respectively. It can be seen in Figures 7.1 & 7.2 that there does appear to be a general trend between SHARE soil moisture and ET_0 in particular with soil moisture being high when ET_0 is low and *vice versa*; however, there are quite a few outliers. A trend corresponding to rainfall is more difficult to detect.

A



B

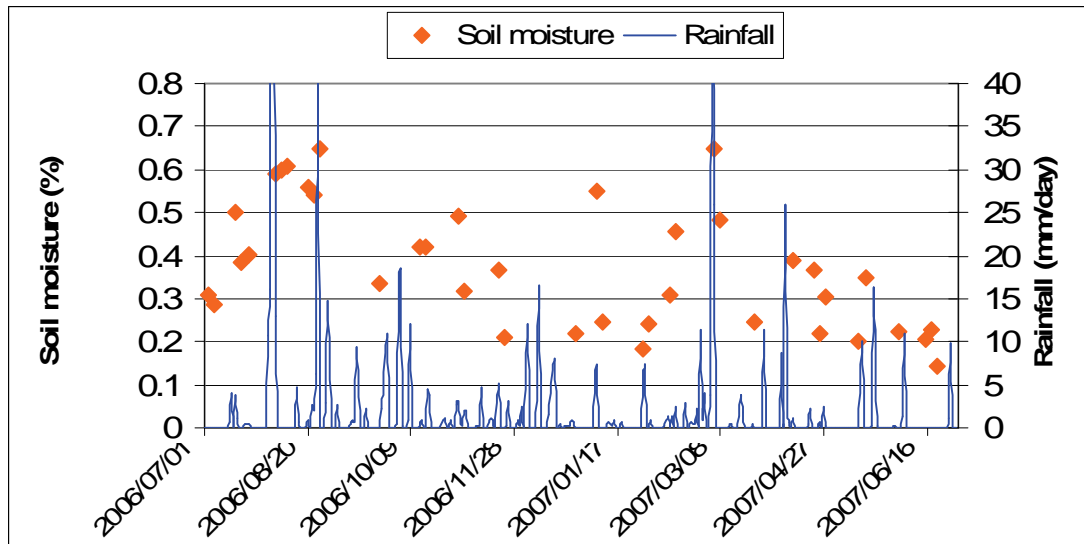
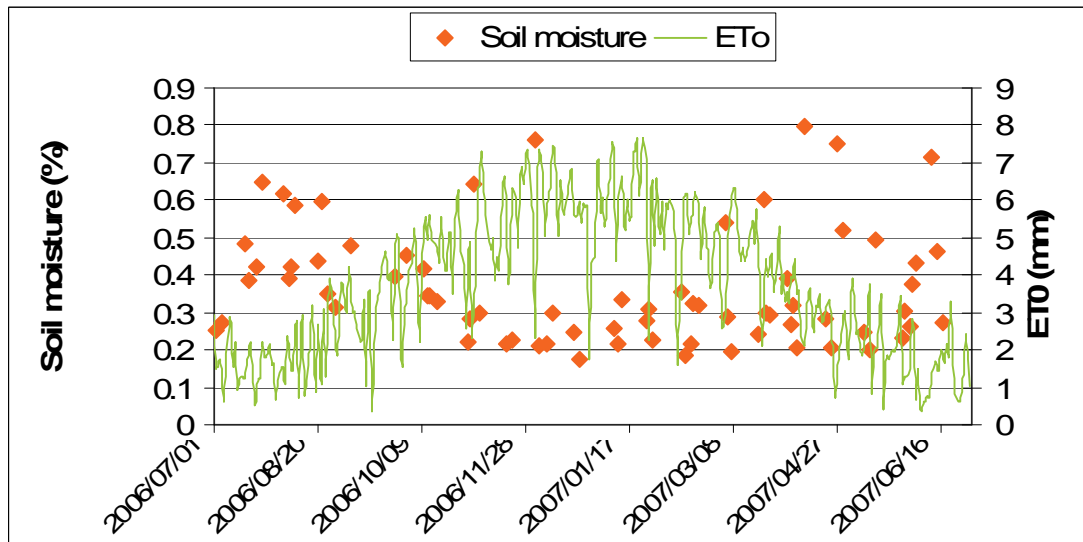


Figure 7.1: SHARE soil moisture data plotted against rainfall for G30G (A) and P10A (B)

A



B

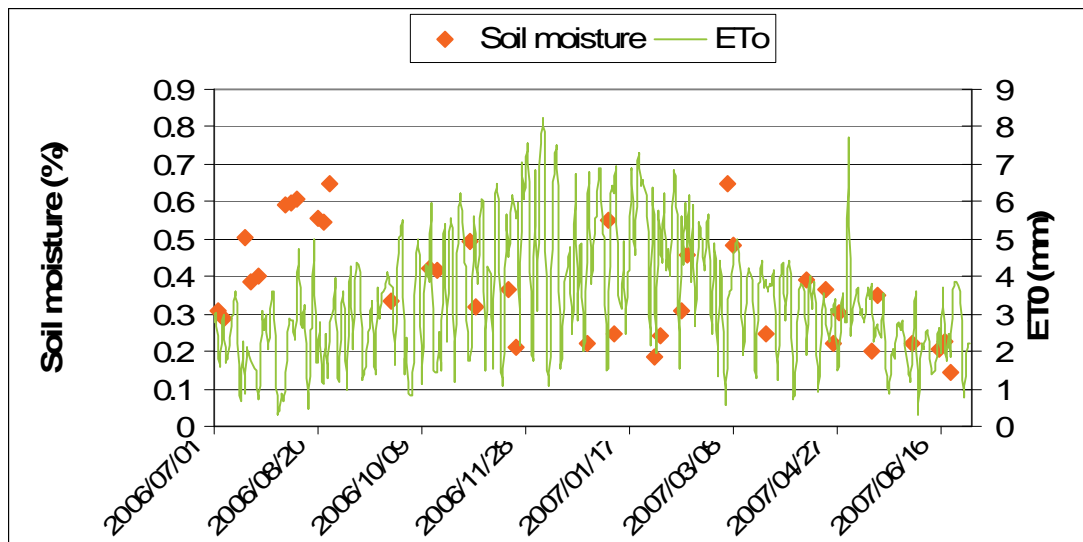


Figure 7.2: SHARE soil moisture data plotted against ET_0 for G30G (A) and P10A (B)

In an attempt to remove outliers, the median of the monthly averages was selected as a representative soil moisture value for a catchment. The value of doing such an exercise is debatable given the high variability of soil moisture in space and time, but as a first attempt to use the SHARE data, it is of interest to see results of some description. In particular instances such as where high rainfall occurred early in the month but the median soil moisture value fell at the end of the month will make it difficult to draw hard conclusions regarding the applicability of the soil moisture dataset to a study such as this. However, the rationale behind using the SHARE dataset was to further confirm fluctuations in the water balance at catchment scale in a

qualitative rather than quantitative manner. The median monthly soil moisture values and the number of datasets used for the median calculation are shown for G30G and P10A in Figures 7.3 & 7.4 respectively. In G30G, the lowest confidence is in the September 2006 value where only two datasets were processed and in P10A, the lowest confidence is in September and December 2006 values where only one dataset was processed for these months. In general, there is a lower confidence in the P10A results since fewer datasets were used to extract the median value.

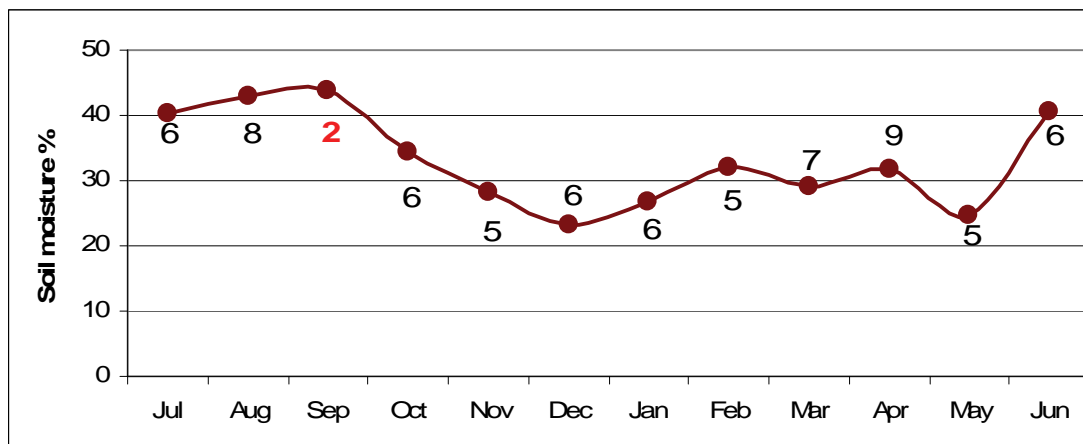


Figure 7.3: Median soil moisture values in G30G. Labels indicate the number of datasets used to extract the median value for each month

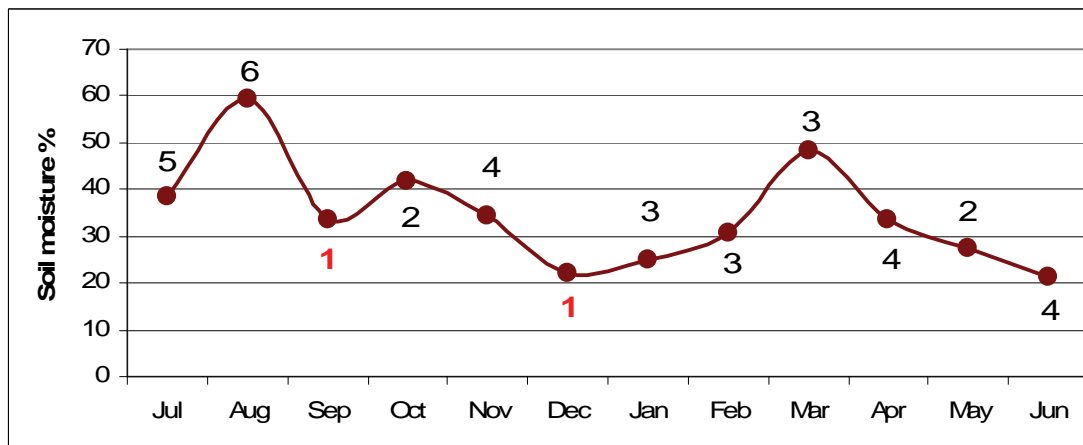


Figure 7.4: Median soil moisture values in P10A. Labels indicate the number of datasets used to extract the median value for each month

Chapter 8 – Runoff

G30G

The Jakkals River that drains the G30G catchment is a non-perennial river which has not been hydrologically mapped. There are many storage dams in the upper reaches of the Jakkals River, both in-channel and off-channel storage dams. River flow to the coastal systems is delayed in the winter rain season as the in-channel dams are first filled before water flows into the next downstream impoundment to eventually reach the coast, if the rain season persists long enough. The coastal Jakkalsvlei is a small, narrow seasonal vlei (coastal lake ~ 0.5 km x 1.4 km) that used to flow via a small estuarine linkage to the sea north of the town of Lamberts Bay. The linkage to the sea was closed for many years by the construction of a berm across the outlet. Recently, however, this berm has been removed to allow the system to function more naturally. There are no significant natural springs within the catchment.

The Department of Water Affairs (DWA) has only two river flow gauging stations within the G30 tertiary catchment: G3H001 at Tweekuilen on the Kruis River and G3H005 at Wittewater on the Hol River. To understand the relationship between runoff and other water balance components, the data from the Tweekuilen river gauge (Figure 8.1) spanning the period April 1970 to May 2009 was investigated. It was found that even though the records indicate availability, the collected data contains no data values with an error code from April 2007. Monthly volumes (in Mm^3 per month) for part of the study period are available and plotted against the catchment average monthly rainfall collected from the ARC-ISCW rainfall grids. From Figure 8.1, the runoff response to rainfall is clear, while the absence of rainfall in the summer months is mirrored by the absence of runoff, with no response to the small rainfall events in February and March 2007. The data collection ended abruptly in April 2007 so the response to the large rainfall event in that month cannot be seen in Figure 8.1.

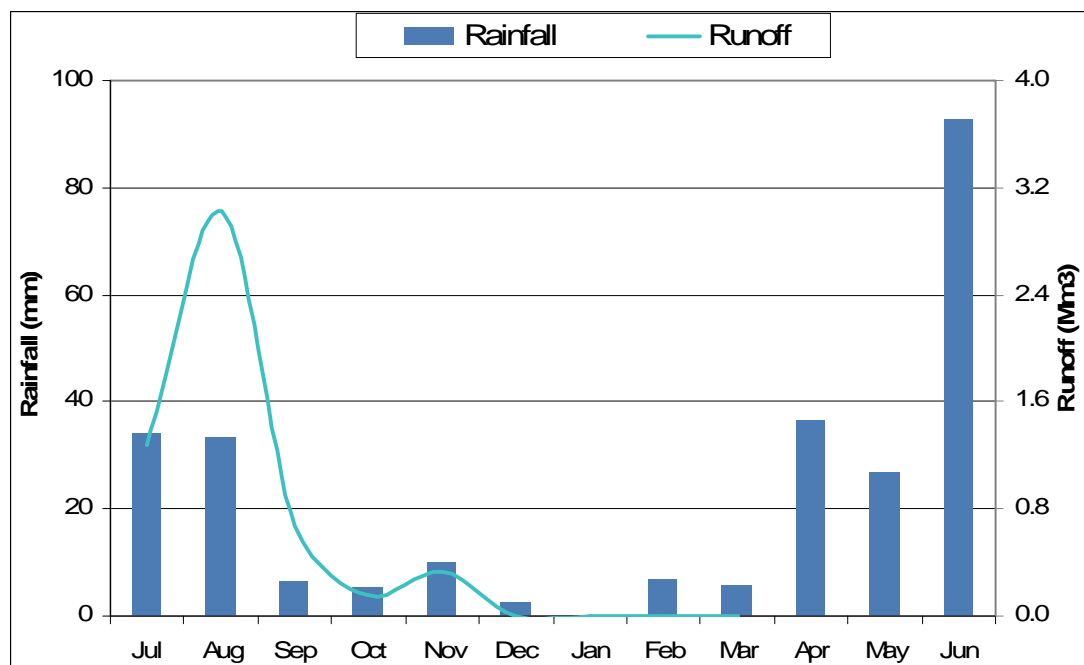


Figure 8.1: G30G runoff at G3H001 Tweekuilen versus rainfall

P10A

As with G30G, no runoff data was available for the P10A catchment. Flow gauging stations existed on the Gxeto (P1H001) and Thorn (P1H002) rivers up to the 1950s. The flow gauging stations on the Boesmans River at Donkerhoek (P1H003) are still in existence collecting data since 1957. Monthly flow gauging data for the period July 2006 to June 2007 available from the DWAF HIS system (<http://www.dwaf.gov.za/Hydrology/>) was plotted against monthly gridded catchment average rainfall (Figure 8.2). It can be seen that the river flow only increases after a substantial rainfall event as experienced in August 2006, but remains predominantly low during the summer months ($< 0.045 \text{ Mm}^3$ per month), rising to only 0.077 Mm^3 as a result of the >90 mm rainfall received during March 2007.

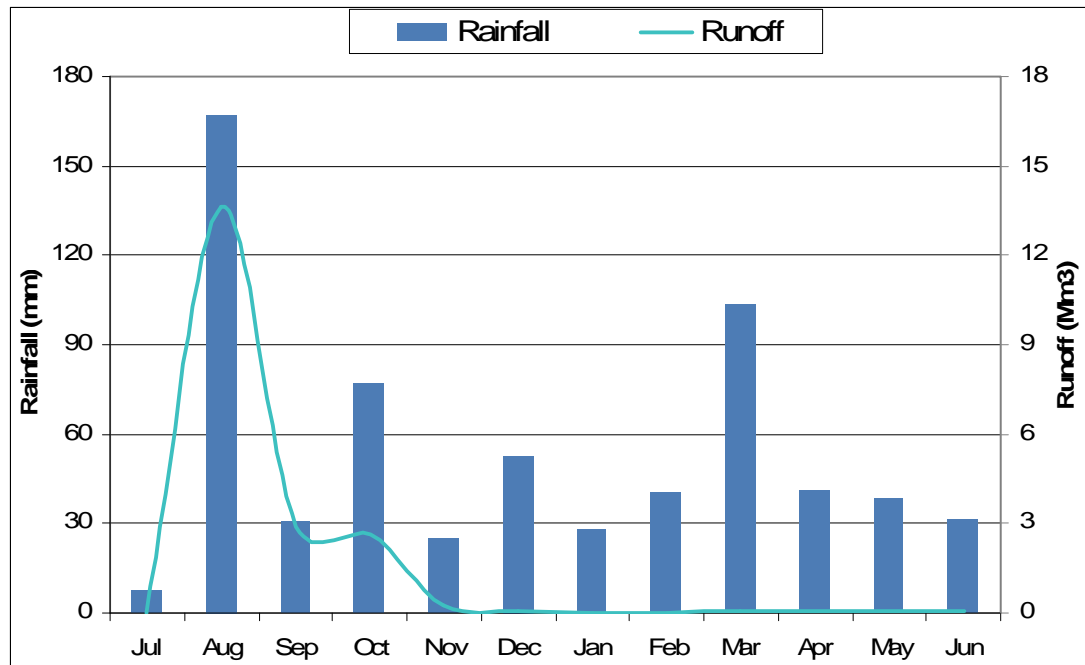


Figure 8.2: P10A runoff at P1H003 Boesmansrivier versus rainfall

Chapter 9 – Water balance

A time series of the independently calculated water balance components shows the fluctuation over time at catchment scale. These interactions will be described.

G30G

For this particular year, the typical rainfall pattern of the study area is apparent with very little rain falling in the hot summer months and consistent rain falling in the winter months with a heavy rainfall month at the end of the study period in June 2007. In Figure 9.1 the results of all the water balance components are shown with the exception of runoff which was excluded due to the incomplete record and the fact that the gauge was located outside the G30G catchment.

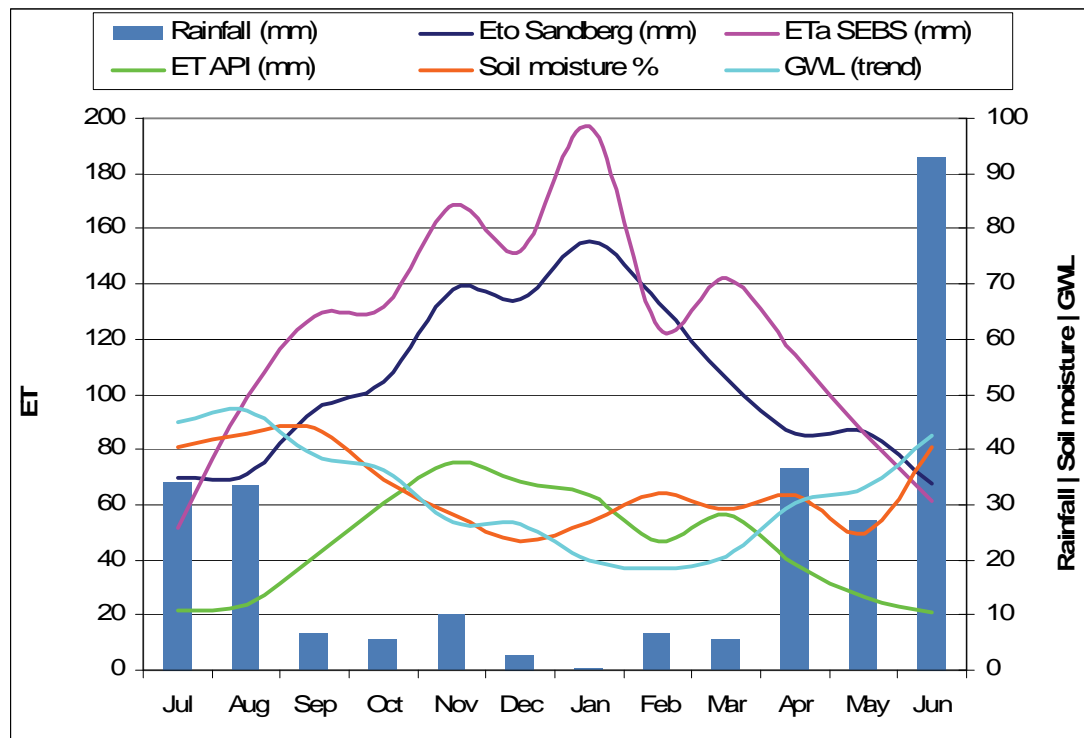


Figure 9.1: G30G water balance

The groundwater level (GWL) shown in Figure 9.1 is not a real value but is rather an exaggerated value⁴ to indicate the trend since real values would not be meaningful at the scale of this particular figure. Soil moisture (median of the catchment average) is shown with a potential range from 0-100 as opposed to the decimal fraction shown earlier in Chapter 7. Once again this was to scale the results to Figure 9.1. The rainfall shown in Figure 9.1 is catchment average results from the ARC-ISCW rainfall grids; likewise the *ET* results are catchment average results but *ET₀* is taken from the Sandberg ARC-ISCW weather station.

The overestimation of the SEBS results is once again apparent in Figure 9.1 as it exceeds *ET₀* for almost every month. The improbability of this result can be seen when examining the results of the other water balance components where the limited water availability during the summer months is reflected. Although the amount of *ET* estimated by SEBS is too large, particularly in the summer months, it follows the *ET₀* curve with the exception of February and March 2007. Likewise, the ET-API follows the *ET₀* trend where water is available and peaks in November 2006 after which it levels out and drops off due to limited water availability. However, the ET-API results appear to be within a more realistic range when compared to other water balance components. Furthermore, the effect of available energy (or atmospheric demand) can be seen in all the *ET* results (including *ET₀*) where the *ET* is lowest in the winter months regardless of the high water availability. Assuming the rainfall and ET-API results are accurate, the cumulative rainfall and ET-API for the study period (Figure 9.2) are compared. Figure 9.2 indicates that there is a negative water balance if only these two water balance components are considered, implying that catchment G30G is a net consumer of water for the study period. Although not quantified, the water level results indicate that regional recharge is contributing positively to the catchment water balance. Should recharge not account for the difference between cumulative ET-API and rainfall, the catchment will be experiencing water stress for the study period.

⁴ Groundwater level shown in Figure 9.1 is calculated as $200 - (\text{real groundwater level in mbgl} \times 10)$

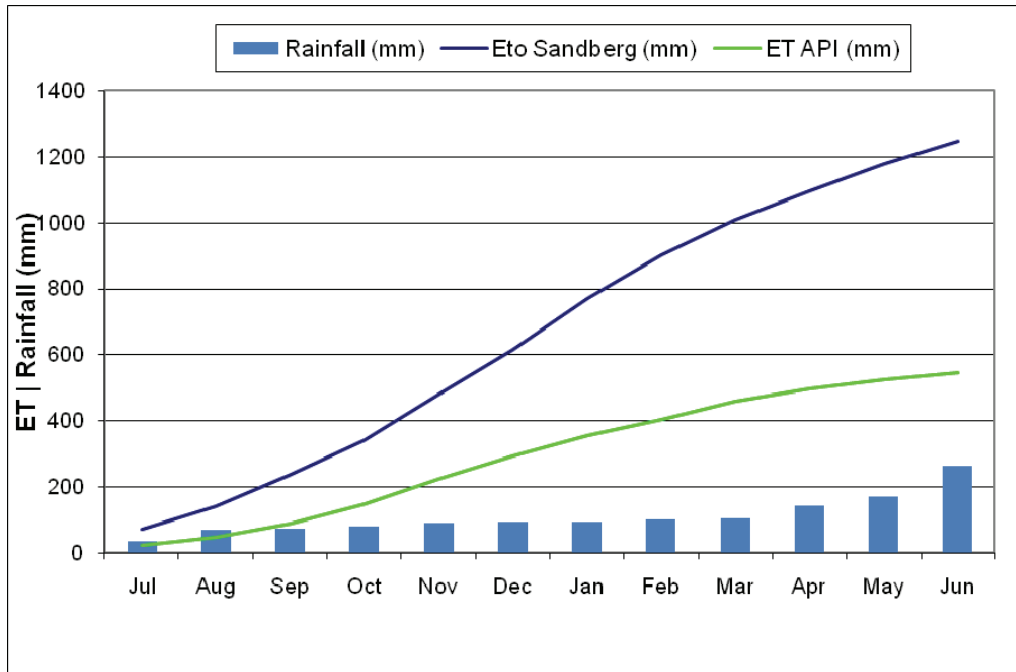


Figure 9.2: G30G cumulative rainfall, ET-API and ET_0

The soil moisture and groundwater level results confirm the water availability, limited in the summer and plentiful in the winter. The correlation between soil moisture and groundwater level is also apparent with February and March 2007 being the exception possibly due to singular rainfall events in the hot dry season. A possible explanation can be that the rainfall events in February and March were enough to wet the soil but not enough to contribute to recharge. The wetting of the soil allowed for a mini peak in ET-API in March (contrary to the downward trend of ET_0) in response to the availability of water. The SEBS result also detected this mini peak.

P10A

For this particular year, the typical rainfall pattern of the study area is apparent with very little rain falling in July 2006 and June 2007 and higher rainfall falling in October 2006 and March 2007. There was an exceptional rainfall event in August 2006. In Figure 9.3 the results of all the water balance components are shown with the exception of runoff which was excluded due to the fact that the gauge was located outside the P10A catchment. There is no groundwater level in Figure 9.3 as none was available for the P10A catchment. As with G30G, (1) soil moisture is shown with a potential range from 0-100 to scale the results to Figure 9.3, (2) the rainfall is

catchment average results from the ARC-ISCW rainfall grids, and (3) the ET results are catchment average results but ET_0 is taken from the Rockhurst ARC-ISCW weather station.

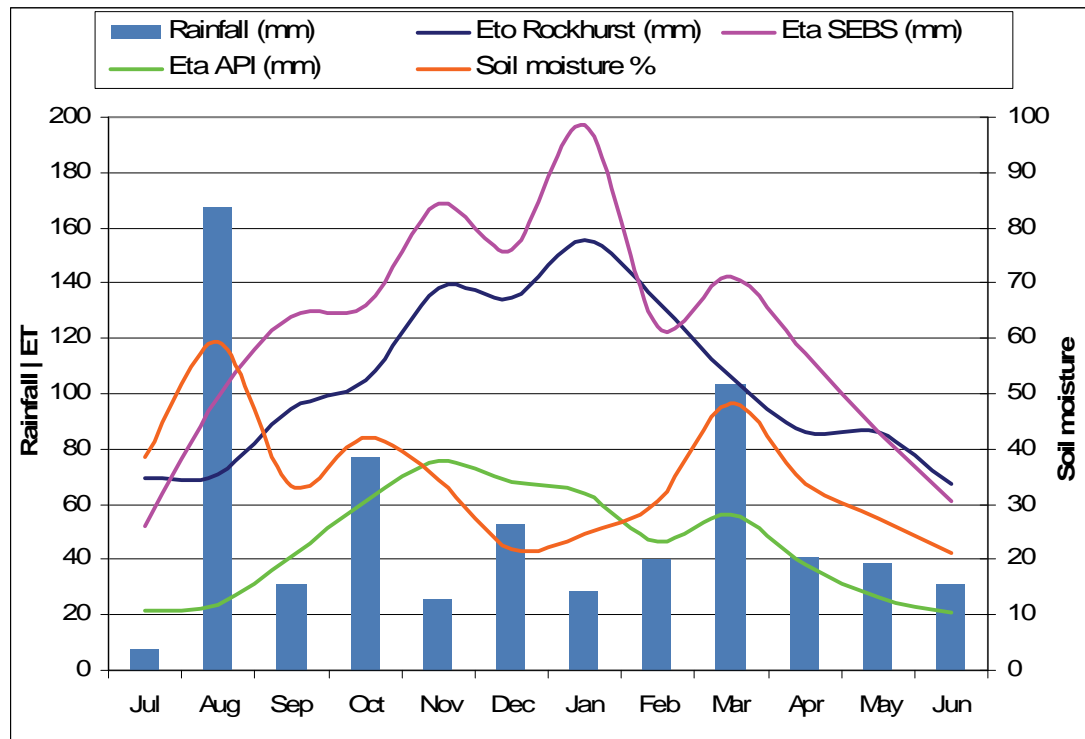


Figure 9.3: P10A water balance

Although Figure 9.3 again demonstrates that the amount of ET estimated by SEBS is too high, particularly in the summer months, it follows the ET_0 curve with the exception of February 2007. Both the SEBS ET and the ET-API results show the response to the rainfall in March 2007 showing a mini peak in this month. Once again the ET-API results appear to be within a more realistic range when compared to other water balance components and as with G30G, the effect of available energy can be seen in all the ET results (including ET_0) where the ET is lowest in the winter months regardless of the water availability. As with G30G, the cumulative rainfall and ET-API for the study period (Figure 9.4) are compared. In contrast to G30G, Figure 9.4 indicates that there is a positive water balance if only these two water balance components are considered, implying that catchment P10A is a net producer of water for the study period. It is assumed that the difference between cumulative ET-API and rainfall would contribute to runoff and exit the catchment, thereby contributing to the Boesmans River downstream.

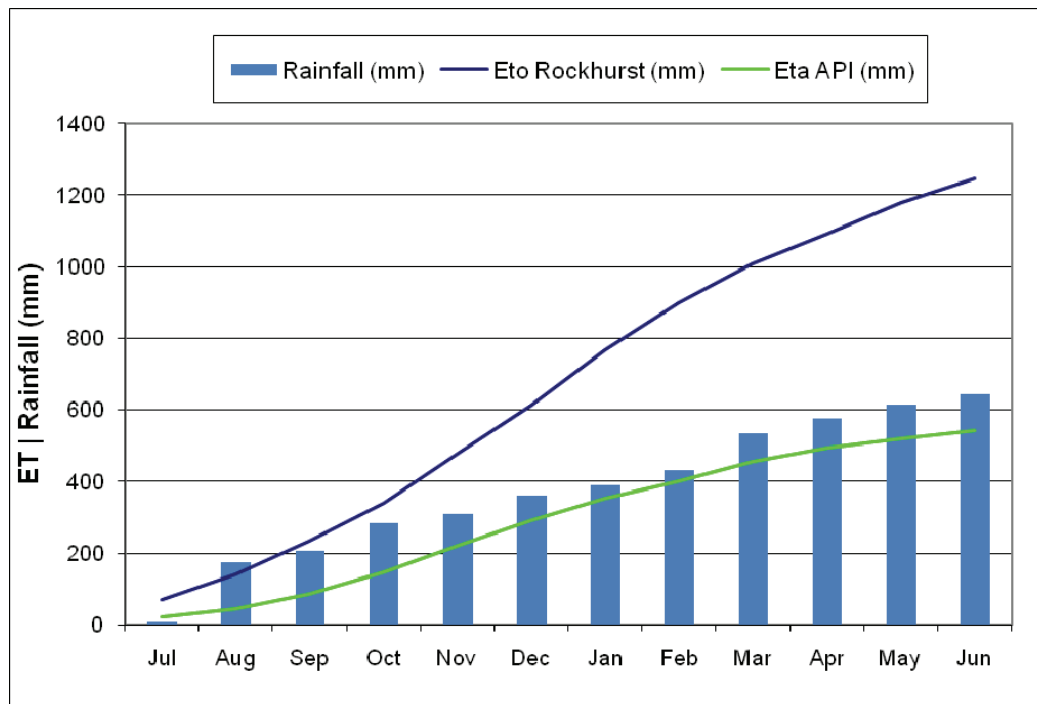


Figure 9.4: P10A cumulative rainfall, ET-API and ET_0

Due to the lower number of datasets available in P10A (see Figure 7.4), there is lower confidence in the soil moisture results. Nevertheless, the response of soil moisture to rainfall can be seen particularly in August 2006. The non-response of soil moisture to rainfall in December 2006 can be ascribed to the fact that there was only one dataset available in that month.

Chapter 10 – Conclusions and Recommendations

Conclusions

Even though this project investigated various water balance components, the main focus was on the accurate calculation of ET using the SEBS model and remote sensing input data. Despite the modifications to reduce uncertainties, as with the results of Gibson *et al.* (2009), the SEBS model appears to overestimate catchment ET. In most cases the SEBS ET results do not appear to reflect limits in water availability and ET is simply highest when the energy or atmospheric demand is the highest and lowest where the energy or atmospheric demand is the lowest. Regardless of the accuracy of the input data (excluding image resolution), the hydrological regime and the environment, the results indicate that the SEBS model remains unable to allocate enough energy to the sensible heat flux (H), leading to an overallocation of energy to the latent heat flux and therefore an overestimation of ET. It is believed that the overestimation in ET is caused by the sensitivity of H to $T_o - T_a$ and z_o , both separately and in combination, particularly at high $T_o - T_a$ and z_o . This sensitivity to $T_o - T_a$ is particularly important with respect to image selection, including the time of day of image acquisition, as the differential heating of the land surface and the air will determine the magnitude and sign of $T_o - T_a$.

New research by Timmermans *et al.* (2011) has indicated that “the uncertainties in the sensible heat flux arise due to a misparameterization of the roughness height for heat. In the original SEBS formulation the roughness height for heat is only valid for short vegetation.” This finding, based on research conducted in a maize field (Timmermans *et al.*, 2011) may help in the reduction of H but further investigations would be needed to establish this in natural or mixed vegetation.

An alternative method to calculate ET from remotely sensed data referred to as the ET-API method returned more realistic results for both the G30G and P10A catchments but in the absence of field validation data the absolute accuracy of this model could not be determined. The trend of the ET-API method over the study period was more favourable in that it reflected both the availability of energy and the availability of water with peaks in precipitation during the dry season being reflected in the ET-API results.

The ARC-ISCW rainfall grid produced results which were positive when validated against rain gauges which were not used in the construction of the grid. For both the G30G and P10A catchments, the best correlations occurred in the months with the highest rainfall. Although the availability of validation results was limited, the ARC-ISCW grid appears to predict catchment rainfall with a high degree of accuracy.

The groundwater results for the G30G catchment accurately reflected the effect of rainfall on recharge, despite the limited groundwater data that were available. The high *ET* results despite low rainfall in the summer months indicate that water may be available from local recharge.

The SHARE soil moisture data was used in a rather crude method to indicate its usefulness in a study of this nature. It was found that there is a general trend between SHARE soil moisture and *ET₀* in particular with soil moisture being high when *ET₀* is low and *vice versa*, however, a few outliers were detected. When using median monthly values, the SHARE soil moisture results displayed an inverse relationship to ET-API, particularly in G30G. The correlation of SHARE results to water levels was also noted in G30G. In P10A, where there were fewer SHARE datasets available, the results were not as striking as in G30G but in both catchments the response of SHARE soil moisture to rainfall events was noted.

Runoff was not used in the water balance due to the difficulty in finding gauged catchments with complete data records. The shortage of gauged catchments is a challenge in water balance studies at quaternary catchment scale.

The response of the differing water balance components over the study period showed that the results of the different methodologies agree in terms of the trends that they highlight. However, the results were not used in a quantitative manner to determine an actual water balance or water stress for a catchment, although from the cumulative rainfall and *ET* results in G30G, the higher than rainfall *ET* results could indicate water stress. From this study it can be concluded that *ET* (ET-API) and precipitation methodologies presented may be used quantitatively for a water balance study at quaternary catchment scale. Soil moisture, which gives an indication of the relative soil moisture rather than a quantity of water stored in the soil, can be used to assess the

reliability of the ET results by indicating the availability of water. Water levels where available are more difficult to incorporate since they represent point locations and are not necessarily representative of a catchment. Finally, the shortage of river gauges makes the incorporation of runoff data difficult.

Recommendations

The estimation of catchment *ET* using the SEBS model was unrealistically high. With the recent publication by Timmermans *et al.* (2011), the possibility for repeating the exercise with the improved parameterization exists. Given the open-source freeware nature of the SEBS model it is recommended that a small test of the new model is run on a limited amount of data. It will be very quickly established whether or not the new version is addressing the particular issues contributing to the underestimation of *H* in the SEBS model used by the project team. If this does not resolve the issues, the use of SEBS in natural vegetation in South Africa is not recommended; however, the application in irrigated agriculture may still be explored.

The ET-API method should receive additional research effort. There are still some concerns regarding the optimized scaling factor which relates leaf-level conductance to canopy conductance which needs to be addressed; however, the results in both the G30G and P10A catchments were promising. The method should also be tested on a pixel by pixel basis for a study of this nature rather than simply using catchment average values.

Other aspects raised in the SEBS *ET* results which are not unique to the SEBS model and are also factors in other energy balance models should be tackled. Research into the influence of time of day of satellite acquisition on land surface air temperature gradient and how this impacts on daily *ET* results should be looked at to determine whether morning or afternoon acquisitions are most suitable for studies of this nature. A methodology to produce accurate roughness lengths is also required. The methodology would need to reflect the changing nature of the vegetation throughout the year and the phenological cycles of particular land covers would need to be taken into account. Perhaps roughness length tables for particular land covers on the basis of NDVI could be set up and incorporated into models such as the SEBS model.

Finally the SHARE soil moisture data was shown to have some application when used at catchment scale and an assessment of its applicability at pixel scale to determine intra-catchment soil moisture and *ET* variability would be useful.

References:

- Alvarez, J.A.G., 2007. Effects of land cover changes on the water balance of the Palo Verde Wetland, Costa Rica, M.Sc. thesis, International Institute for Geo-information Science and Earth Observation, The Netherlands.
- ARC-ISCW, 2005. Ten Daily Rainfall Estimate Grids. Grid metadata
- ARC-ISCW, 2010. Technical manual for the AgroClimatology Weather Station Network. ARC-ISCW internal report, Agricultural Research Council-Institute for Soil, Climate and Water, South Africa, Report No. GW/A/2008/60.
- Badola, A., 2009. Validation of Surface Energy Balance System (SEBS) over forest land cover and sensitivity analysis of the model, M.Sc. thesis, International Institute for Geo-information Science and Earth Observation, The Netherlands.
- Bastiaanssen, W.G.M., Menenti, M., Feddes, R.A. & Holtslag, A.A.M., 1998. The Surface Energy Balance Algorithm for Land (SEBAL): Part 1 formulation., *Journal of Hydrology*, 212-213: 198-212.
- Batelaan, O. & De Smedt, F., 2001. WetSpass: a flexible, GIS based, distributed recharge methodology for regional groundwater modelling. In: Gehrels, H., Peters, J., Hoehn, E., Jensen, K., Leibundgut, C., Griffioen, J., Webb, B. & Zaadnoordijk, W-J. (eds). *Impact of Human Activity on Groundwater Dynamics*. IAHS Publ. no. 269, Wallingford UK, pp11-17.
- Brutsaert, W., 1982. *Evaporation into the atmosphere*, Reidel, Dordrecht, The Netherlands, 299 pp.
- Carlson, T.N. & Ripley, D.A., 1997. On the relation between NDVI, Fractional Vegetation Cover, and Leaf Area Index, *Remote Sensing of Environment*, 62: 241-252.
- Choudhury, B.J., 1987. Relationships between vegetation indices, radiation absorption, and net photosynthesis evaluated by a sensitivity analysis. *Remote Sensing of Environment*, 22: 209-233.
- De Beer, C., 2003. The geology of the Sandveld area between Lambert's Bay and Piketberg (Project 5510). Council for Geoscience, Western Cape Unit.
- Doubkova, M., Bartsch, A., Pathe, C., Sabel, D. & Wagner, W., 2009. The medium resolution soil moisture dataset: overview of the SHARE ESA DUE TIGER project, *International Geoscience and Remote Sensing Symposium (IGARSS)*, art. no. 5416930, pp. I116-I119.
- Flores, A.N., Ivanov, V.Y., Entekhabi, D. & Bras, R.L. 2009. Impact of Hillslope-Scale Organization of Topography, Soil Moisture, Soil Temperature, and Vegetation on Modeling Surface Microwave Radiation Emission. *IEEE Transactions on Geoscience and Remote Sensing*, 47(8): 2557-2571.

Gebreyesus, M.G., 2009. Validation of RS approaches to model surface characteristics in hydrology: a case study in Guareña Aquifer, Salamanca, Spain, The Netherlands, M.Sc. thesis, International Institute for Geo-information Science and Earth Observation, The Netherlands.

Gellens-Meulenberghs, F., 2005. Sensitivity tests of an energy balance model to choice of stability functions and measurement accuracy. *Boundary-Layer Meteorology* 115: 453-471.

GEOSS, 2006. Groundwater Reserve determination required for the Sandveld, Olifants Doorn Water Management Area, Western Cape, South Africa. Prepared for the Department of Water Affairs and Forestry, Pretoria. Prepared by GEOSS, Stellenbosch.

Gibson, L.A., Münch, Z., Engelbrecht, J., Petersen, N. & Conrad, J.E., 2009. Remote sensing as a tool towards resource assessment and determination of the legal compliance of surface and groundwater use. WRC Project K5/1690. Water Research Commission, Pretoria.

Gibson, L.A., Münch, Z., Engelbrecht, J. & Conrad, J., 2010. Uncertainties in using remote sensing for water use determination: a case study in a heterogeneous study area in South Africa. *Hydrology and Earth System Sciences Discussion*, 7: 6581-6612.

Gibson, L.A., Münch, Z., & Engelbrecht, J., 2011. Particular uncertainties encountered in using a pre-packaged SEBS model to derive evapotranspiration in a heterogeneous study area in South Africa. *Hydrology and Earth System Sciences*, 15: 295-310.

Gutman, G. & Ignatov, A., 1998. The derivation of the green vegetation fraction from NOAA/AVHRR data for use in numerical weather prediction models, *International Journal of Remote Sensing*, 19: 1533-1543.

Hailegiorgis, W.S., 2006. Remote sensing analysis of summer time evapotranspiration using SEBS algorithm: a case study in Regge and Dinklel, The Netherlands, M.Sc. thesis, International Institute for Geo-information Science and Earth Observation, The Netherlands.

Jia, L., Su, Z., Van den Hurk, B., Menenti, M., Moene, H.A.R., Baselga Yrisarry, J.J., Ibanez, M. & Cuesta, A., 2003. Estimation of sensible heat flux using the Surface Energy Balance System (SEBS) and ATSR measurements, *Physics & Chemistry of the Earth*, 28: 77-88.

Kipp & Zonen, 2005. Large Aperture Scintillometer instruction manual. Delft, Holland.

Kustas, W.P., Li, F., Jackson, T.J., Prueger, J.H., MacPherson, J.I., & Wolde, M., 2004. Effects of remote sensing pixel resolution on modeled energy flux variability of croplands in Iowa. *Remote Sensing of Environment*, 92(4): 535-547.

Lin, W., 2006. Satellite based regional scale evapotranspiration in the Hebei Plain, Northeastern China, The Netherlands, M.Sc. thesis, International Institute for Geo-information Science and Earth Observation, The Netherlands.

Li, Z., Yu, G., Li, Q., Fu, Y. & Li, Y., 2006. Effect of spatial variation on areal evapotranspiration simulation in Haibei, Tibet plateau, China. *International Journal of Remote Sensing*, 27(16): 3487-3498.

- Li, F., Kustas, W.P., Anderson, M.C., Prueger, J.H. & Scott, R.L., 2008. Effect of remote sensing spatial resolution on interpreting tower-based flux observations, *Remote Sensing of Environment*, 112: 337-349.
- McCabe, M.F. & Wood, E.F., 2006. Scale influences on the remote estimation of evapotranspiration using multiple satellite sensors, *Remote Sensing of Environment*, 105: 271-285.
- McCabe, M.F., Wood, E.F., Wójcik, R., Pan, M., Sheffield, J., Gao, H. & Su, H., 2008. Hydrological consistency using multi-sensor remote sensing data for water and energy cycle studies, *Remote Sensing of Environment*, 112: 430-444.
- Middleton, B.J. & Bailey, A.K., 2008. Water resources of South Africa, 2005 STUDY (WR2005). WRC Contract K5/1491. Water Research Commission, Pretoria, South Africa.
- Mucina, L and Rutherford, M.C. (eds), 2004. Vegetation Map of South Africa, Lesotho and Swaziland: shape files of basic mapping units. Beta version 4.0, February 2004. National Botanical Institute, Cape Town.
- Palmer, A.R. & Weideman, C.I., 2011. Exploring trends in evapotranspiration in the KNP: towards a water use efficiency model for rangeland production in semi-arid savannas. Proceedings of the IXth International Rangeland Congress, Rosario, Argentina. 2-8 April 2011.
- Pan, M., Wood, E.F., Wójcik, R. & McCabe, M.F., 2008. Estimation of regional terrestrial water cycle using multi-sensor remote sensing observations and data assimilation, *Remote Sensing of Environment*, 112, 1282-1294.
- Rahman, H. & Dedieu, G., 1994. SMAC: a simplified method for the atmospheric correction of satellite measurements in the solar spectrum. *International Journal of Remote Sensing*, 15(1): 123-143.
- Sobrino, J.A. & El Kharraz, J., 2003. Surface temperature and water vapour retrieval from MODIS data, *International Journal of Remote Sensing*, 24, 5161-5182.
- Su, Z., 2002. The surface energy balance system (SEBS) for estimation of turbulent heat fluxes, *Hydrology and Earth System Sciences*, 6: 85-99.
- Su, Z., 2006. An introduction to the surface energy balance system (SEBS), Lecture notes, ESA TIGER Capacity Building Facility 1st Training Course on “Advanced optical remote sensing”, Cape Town, 22-25 November 2006.
- Su, H., McCabe, M.F. & Wood, E.F., 2005. Modeling Evapotranspiration during SMACEX: Comparing Two Approaches for Local- and Regional-Scale Prediction, *Journal of Hydrometeorology – Special Section*, 6: 910-922.
- Su, Z. & Roerink, G.J. (editors), 2004. Drought Risk Reduction, Wageningen, Alterra, Alterra-rapport 1135.

Timmermans, W.J., Van der Kwast, J., Gieske, A.S.M., Su, Z., Oliso, A., Jia, L. & Elbers, J. , 2005. Intercomparison of energy flux models using ASTER imagery at the SPARC 2004 site, Barrax, Spain, in: Proceedings of the ESA WPP-250: SPARC final workshop, Enschede, 4-5 July 2005, 8 p.

Timmermans, J., Van der Tol, C., Verhoef, A., Verhoef, W., Su, Z., Van Helvoirt, M. & Wang, L., 2011. Quantifying the uncertainty in estimates of surface- atmosphere fluxes through joint evaluation of the SEBS and SCOPE models. *Hydrology and Earth System Sciences Discussion*, 8: 2861-2893.

Van den Berg, E.C., Plarre, C., Van den Berg, H.M. & Thompson, M.W. , 2008. The South African National Land Cover 2000. Agricultural Research Council-Institute for Soil, Climate and Water, Pretoria, Report GW/A/2008/86.

Van der Kwast, J., Timmermans, W., Gieske, A., Su, Z., Oliso, A., Jia, L., Elbers, J., Karssenberg, D. & De Jong, S. , 2009. Evaluation of the Surface Energy Balance System (SEBS) applied to ASTER imagery with flux-measurements at the SPARC 2004 site (Barrax, Spain), *Hydrology and Earth System Sciences*, 13, 1337-1347.

WR90. Water Resources of South Africa 1990 (WR90). Published by the Water Research Commission, Pretoria.

Xiong, X., Sun, J., Esposito, J., Guenther, B. & Barnes, W. 2002. MODIS Reflective Solar Bands Calibration Algorithm and On-orbit Performance. Available on line at URL: http://mcst.gsfc.nasa.gov/uploads/files/SPIE_CHINA_RSB.pdf

APPENDIX 1 – P10A field campaign

WRC project K8/929/1 Field trip to Grahamstown 12-14 October 2010

The field trip to Grahamstown for the purpose of visiting quaternary catchment P10A (study area for summer rainfall area) was undertaken in October 2010. The objective of the visit was to give the researchers the opportunity to view the landscape and evaluate the landcover classification (NLC 2000) as well as parameters determined using the SEBS model. It was also an opportunity to meet with Dr Tony Palmer from the ARC in Grahamstown, and his team, who are responsible for collecting data in the Grahamstown area which can be used to validate the results of this study. The NLC 2000 as well as the extent of the study area is shown in Figure A1.

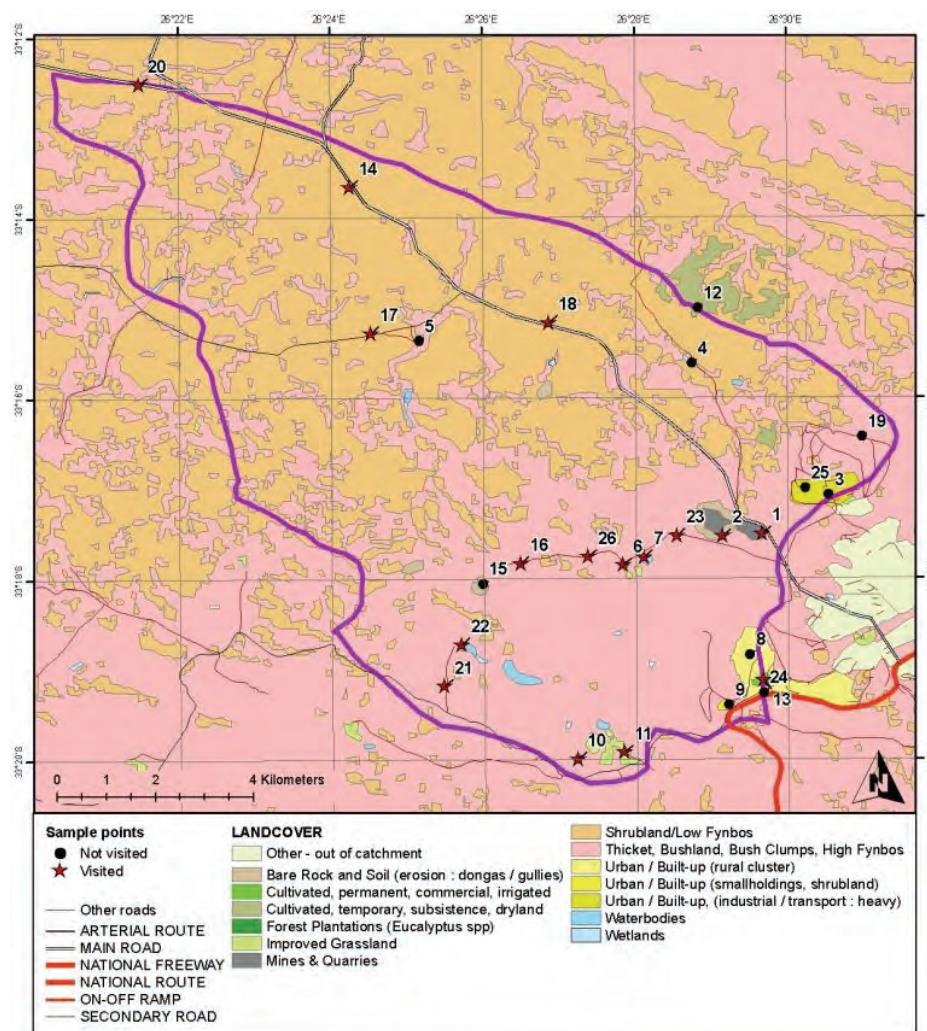


Figure A1: Map of sites to visit for field sampling of ET

Figure A2 gives an overview of the northern part of the catchment, drier with small bushes, predominantly classified as *Shrubland* and *Low Fynbos* in the NLC (Figure A1). The southern part of the catchment is dominated by thicker vegetation, classified as *Thicket*, *Bushland*, *Bush Clumps*, *High Fynbos*, as can be seen in Figure A3.



Figure A2: Northern part of study area looking south from sample point 14



Figure A3: Southern part of study area, more thickly vegetated

Twenty-five sampling sites were selected randomly with at least one sample per landcover class in the study area with the dominant classes each having at least 4 sampling points. The location of all selected sampling sites, visited or not, is shown in Figure A1 and Table A1 which also lists NLC 2000 landcover classification per site. The sites were visited by a team representing ARC-API Grahamstown, GEOSS, SU and ARC-ISCW (Figure A4). At the outset it was decided that the class representing urban would not be visited. During the trip an additional sampling site was added, which appeared to accurately represent the class *Thicket*, *Bushland*, *Bush Clumps*, *High Fynbos*, numbered 26. Additionally the airport site was visited where the Grahamstown weather (rainfall) station is located. Canopy height measurements were done by the ARC-API Grahamstown team during a capacity building exercise.

The protocol followed at each sampling site is listed below:

- Note the number of the sampling point, time and NLC landcover classification
- Obtain local knowledge (if any) from Dr Tony Palmer and take measurements if required
- Take four photographs – to north, east, south and west, subject faces north
- Extract SEBS parameters for day of year 2005-185 from GIS database and list Evapotranspiration (ET), fractional vegetation cover (FC), canopy height scene specific (CHs), canopy height time-series derived (CHt) and Normalized Difference Vegetation Index (NDVI)

Results according to protocol from the field visit can be found in Table A2. For each site the four photographs are displayed in a single row ordered north, east, south and west. Additional photographs taken are annotated and placed in a separate row. The parameters extracted from remote sensing data using SEBS or other processing and placed in the GIS database for the study area, are depicted in Figure A5.





Table A1: Landcover types according to National Land Cover 2000 dataset for field sampling sites





Id	Landcover Type	Lat	Long	X	Y
1	Mines & Quarries (surface-based mining)	-33.291855	26.494411	-47092.9900	-3685230.8983
2	Bare Rock and Soil	-33.292254	26.485633	-47910.3905	-3685279.1451
3	Urban/Built-up, (industrial/transport: heavy)	-33.284667	26.508845	-45752.2550	-3684427.2349
4	Wetlands	-33.260371	26.478982	-48547.5763	-3681746.0298
5	Improved Grassland-borders on cultivated (N,topo)	-33.256094	26.419215	-54119.2912	-3681301.0262
6	Improved Grassland	-33.297555	26.463884	-49933.1938	-3685877.2734
7	Waterbodies	-33.296148	26.468416	-49511.9111	-3685719.0398
8	Urban / Built-up (rural cluster)-border cultiv	-33.314111	26.491529	-47349.3686	-3687700.5842
9	Urban / Built-up (smallholdings, shrubland)	-33.323428	26.486827	-47782.2276	-3688736.1887
10	Forest Plantations (Eucalyptus spp)	-33.333394	26.453840	-50847.9272	-3689857.1229
11	Improved Grassland	-33.332138	26.464020	-49900.8446	-3689712.8981
12	Cultivated, temporary, subsistence, dryland	-33.250200	26.480331	-48427.5003	-3680617.3118
13	Cultivated, permanent, commercial, irrigated	-33.318898	26.494531	-47067.3093	-3688230.2281
14	Shrubland and low fynbos	-33.227733	26.404279	-55528.9581	-3678163.2823
15	Bare rock and soil	-33.300944	26.433103	-52798.0982	-3686268.2548
16	Thicket, Bushland, Bush Clumps, High Fynbos	-33.297238	26.441402	-52027.3497	-3685853.1129
17	Shrubland and low fynbos	-33.254727	26.408778	-55092.6497	-3681154.8887
18	Shrubland and low fynbos	-33.252842	26.447842	-51453.5485	-3680925.8253
19	Thicket, Bushland, Bush Clumps, High Fynbos	-33.273916	26.516324	-45061.0925	-3683231.5903
20	Shrubland and low fynbos	-33.208689	26.358206	-59836.6260	-3676076.5615
21	Thicket, Bushland, Bush Clumps, High Fynbos	-33.319838	26.424620	-53576.6411	-3688368.1509
22	Waterbodies	-33.312181	26.428389	-53230.3116	-3687517.0353
23	Thicket, Bushland, Bush Clumps, High Fynbos	-33.292207	26.475693	-48836.3223	-3685278.5211
24	Urban / Built-up (rural cluster)	-33.321149	26.494595	-47060.1437	-3688479.7834
25	Urban/Built-up, (industrial/transport: heavy)	-33.283443	26.503729	-46229.5208	-3684293.7682
26	Thicket, Bushland, Bush Clumps, High Fynbos	-33.296040	26.456260	-50644.1790	-3685712.9026



Figure A4: The ARC-API Grahamstown team, GEOSS, SU and ARC-ISCW

Table A2: Photos, data and local knowledge per field sampling site (in number order)

9:55	Airport Weather station		
Thicket limited to North side, predominantly grassland			
			
10:07	1: Mines & Quarries (surface based mining)		
Kaolin mine used by municipality for dumping. Signal could be influenced by tall gum trees. Golf course to the east of this pixel			
			
ET=7.09 FC=0.39 CHs=1.679 CHt=2.1 NDVI=0.62			
10:24	2: Bare rock and Soil		
This is a mine, surrounded by what looks like unimproved grassland. Canopy low. There may be a borehole here (possibly in the shed)			

			
ET=6.87 FC=0.047 CHs=0.536 CHt=0.66 NDVI=0.38			
3: Urban/Built-up (industrial/transport: heavy)			
Not visited – we decided not to visit any of the urban sites			
4: Wetlands			
Not visited – very small feature, located within Shrubland, low fynbos			
12:30 5: Improved Grassland			
Not visited. Located within homestead of “Table Farm”			
11:05 6: Improved grassland			
Farm – developed. Aloe’s planted			
			
ET=7.32 FC=0.57 CHs=1.83 CHt=2.29 NDVI=0.64			
10:55 7: Waterbodies			
Very dry dam, may have had water in 2006/7			
			
			

			
ET=7.53 FC=0.65 CHs=2.19 CHt=2.75 NDVI=0.69			
	8: Urban / Built-up (rural cluster) 9: Urban / Built-up (smallholdings, shrubland)		
Not visited			
14:43	10: Forest Plantations (Eucalyptus pp)		
There are no tall trees here, only a windbreak along the road, maybe a small woodlot, no photos taken			
ET=7.04 FC=0.879 CHs=2.13 CHt=2.67 NDVI=0.68			
14:23	11: Improved grassland		
Game breeding farm. Houses around the paddock, next to railway line. Very tall trees.			
			
ET=7.04 FC=0.26 CHs=1.55 CHt=1.95 NDVI=0.60			
	12: Cultivated, temporary, subsistence, dryland		
Not visited, almost out of catchment			
15:30	13: Cultivated, permanent, commercial, irrigated		
In the cemetery			
			
ET=7.05 FC=0.26 CHs=1.56 CHt=1.95 NDVI=0.60			
12:18	14: Shrubland and low fynbos		

															
ET=7.13 FC=0.28 CHs=1.1 CHt=1.38 NDVI=0.52															
				15: Bare rock and soil											
Not visited – a previous bare rock and soil site visited															
11:15				16: Thicket, Bushland, Bush Clumps, High Fynbos											
Cultivated on south side of road (from topo) – dryland lucerne / pasture grass. Very tall trees.															
															
								Tall tree measured at 22m							
															
ET=7.12 FC=0.43 CHs=1.5 CHt=1.88 NDVI=0.59															
12:29				17: Shrubland and low fynbos											
Lots of “garingboom” among low bushland															
															
ET=7.13 FC=0.28 CHs=1.1 CHt=1.38 NDVI=0.52															
12:38				18: Shrubland and low fynbos											
Looks like grassland															

	
ET=7.19 FC=0.38 CHs=0.84 CHt=1.05 NDVI=0.46	
19: Thicket, Bushland, Bush Clumps, High Fynbos	
Not visited	
12:05	20: Shrubland and low fynbos
Karoo shrubland. Part of Bushmansriver system. Boreholes on farmer Brown's farm, Brack farm	
	
ET=7.27 FC=0.24 CHs=0.96 CHt=1.19 NDVI=0.49	
21: Thicket, Bushland, Bush Clumps, High Fynbos	
Unimproved grassland. Controlled: Burnt by municipality or farmer. On the way to Milner dam.	
	
ET=7.287 FC=0.313 CHs=0.97 CHt=1.21 NDVI=0.495	
22: Waterbodies	
Very empty Milner dam. Fire damage next to dam. Photos not taken according to protocol	
	
ET=7.3 FC=0.31 CHs=1.12 CHt=1.4 NDVI=0.52	
23: Thicket, Bushland, Bush Clumps, High Fynbos	
Thicket, quite patchy. Regular fires. Patches of grassland close to road, fence. Cattle or kudu (livestock farmer).	

Various trees measured.			
			
	Tree1 = 4 m	Tree2 = ~1.9 m	Tree3 = 3.5m
			
ET=6.87 FC=0.047 CHs=1.6 CHt=2.01 NDVI=0.61			
		24: Urban / Built-up (rural cluster) 25: Urban / Built-up (industrial/transport: heavy)	
Not visited			
11:32		26: Thicket, Bushland, Bush Clumps, High Fynbos	
Mesic thicket according to Tony Palmer. Acacia karoo – good example of thicket New sample point added			
			
ET=7.32 FC=0.57 CHs=1.83 CHt=2.29 NDVI=0.64			

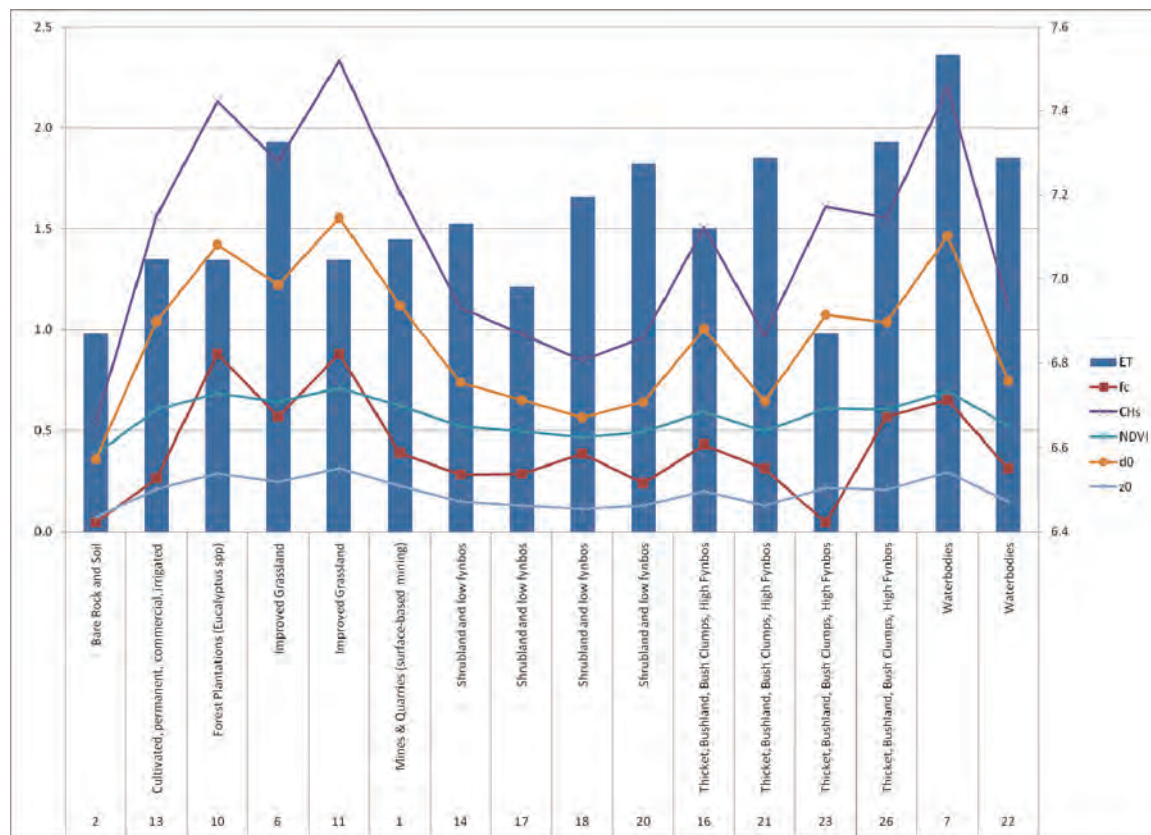


Figure A5: SEBS parameters checked during field visit

Table A3: Hydrocensus results - quaternary catchment P10

ID	BH	Latitude (WGS84)	Longitude (WGS84)	Depth_m	PumpTest Yield	Comments	Water quality
1	Grass camp	-33.22167	26.35333	93.27	441 gal/hr	Drilled March 1970, failed 1983 (Geol: stone and shale)	Good
2	Calf camp	-33.23125	26.38400	17.98	700 gal/hr	Water strikes: 40ft, 50ft and 59ft. Still water in 1990	
3	Yard BH	-33.22713	26.38190	30.48	330 gal/hr	Pump tested in 1948. Still water in 1990	
4	Tottie Camp	-33.23533	26.37000	36.58	60 gal/hr	Drilled 1948. Water strikes: 60ft and 85ft. Still water in 1990	
5	Camp one in vlei	-33.22495	26.35960	89.92		Drilled 1970 (Geol: boulders and Dwyka)	
6	Lands C	-33.22535	26.32553	12.95		Drilled prior to 1906. Fails in drought. Abandoned Feb 1997	
7	Middle C	-33.22448	26.33773	27.43		Drilled 1983 - dry hole	
8	Krantz C	-33.22167	26.32167	90.00	2000 l/hr	Not used	Very Salty, 3500ppm Cl
9	Riebeek	-33.20340	26.34695	60.96		Drilled 1965. Very weak water. Closed 1978	
10	Riebeek Saddle	-33.20447	26.35358	0.00		Drilled 1965. Dry hole.	
11	Springbok Camp	-33.22167	26.38333	9.14		Na:516, Ca: 123, Mg: 106, HCO3: 482, Cl: 1000, hardness: 743, pH: 7.4, EC: 498	
12	Church camp	-33.24105	26.35018	21.95	64 gal/hr		
13	Church camp 2	-33.24158	26.35012	16.36	24 gal/hr	Stopped as very crooked	
15	Tent camp/old b/h	-33.24158	26.35022	0.00		Very weak water	
16	Vlei Camp	-33.20750	26.35750	22.15	30gal/hr	22/2/1946 Dwyka too hard stopped drilling	
17	Hut Camp lands	-33.21833	26.37167	21.95		Only seepage water	
18	New camp	-33.24250	26.38667	48.77	860 gal/hr	Tested 1951	
19	Far camp	-33.25142	26.38162	60.96		Drilled 1951. Site abandoned	
20	Far camp no 2	-33.25077	26.38275	33.53	718 gal/hr	Water strikes: 74ft, 91ft	
21	Hilton land	-33.24717	26.36800				
22	Hilton camp	-33.24727	26.36763				
23	West camp	-33.23980	26.33078			very old hole. Dry	
24	In land Hilton	-33.24717	26.36800			Very weak. Very sulphur rich. John Piek.	
25		-33.24727	26.36763			Casing in hole. J Piek drilled. 300ft deep?	
26	WestC	-33.23972	26.33078			Never used (dry). Below dam	
27	Grass C	-33.22673	26.34022			Drilled 1970. Good water. Failed 1983	Good
28	Camp 1	-33.22840	26.35872			Top near B. Gate. Site selection by Gov. geologist. Drilled 1970. Very deep, but no water. All shale. Approx 400 ft	
29	Camp1_No6	-33.22495	26.35960			Above vlei. Dry. Dwyka.	
32	2nd hole	-33.23298	26.31965		420 l/hr	Near boundary gate in Broxley C in road. Water struck at 6m +/-420lh. Solid tillite to 50m. Discontinued	

33	3rd hole	-33.23160	26.31980		1000-5000 gal/hr	In Broxley C in road near kloof. 1st water strike at 18m 1000 gallons/hr. Successive water strikes every couple of meters. Discontinued at 30m. Total yield estimated 5000 to 1000 Gal/hr. Very fresh water	
34	Broxley Farm	-33.24083	26.31507			Part of Farm Hilton. Owner J White	
35	Hilton House Garden	-33.25115	26.35187				
36	Table Farm W/Mill	-33.25118	26.42278			W/Mill next to road. Old hole. Tillite. +/- 200ft. Good yield	
38	Strowan_BH	-33.29167	26.48611		1000 l/hr	Mike Palmer. Water is brak. Not suitable for irrigation or poultry but OK for livestock.	Brak